Ph. D. DISSERTATION

A Study on the Correlations

between Defects and Light Emitting Characteristics

of GaN-based Light Emitting Devices

using Cathodoluminescence Transmission Electron

Microscopy

투과전자현미경 음극형광 분석을 통한 GaN 기반

소자의 발광특성과 응력과의 상관관계에 대한 연구

by

Sung-Dae Kim

February 2013

Department of Materials Science and Engineering

College of Engineering

Seoul National University

A Study on the Correlations

between Defects and Light Emitting Characteristics

of GaN-based Light Emitting Devices

using Cathodoluminescence Transmission Electron Microscopy

Advisor : Prof. Young-Woon Kim

by

Sung-Dae Kim

A thesis submitted to the Graduate Faculty of Seoul National University
in partial fulfillment of the requirement for
the Degree of Doctor of Philosophy
Department of Materials Science and Engineering

December 2012

Approved

by

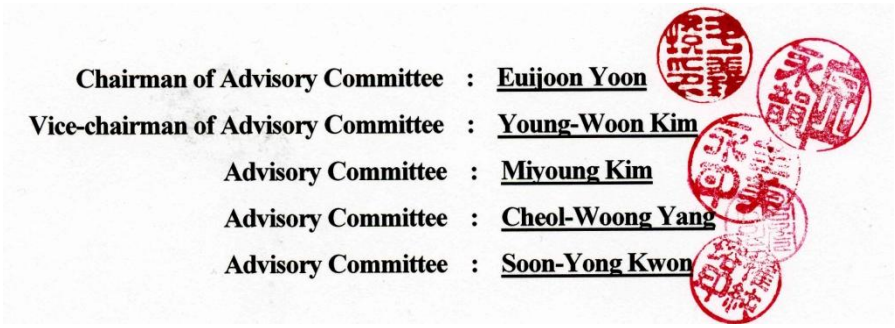

Abstract

As accelerated electron beams interact with materials, various useful signals emitted which have structural, chemical and electrical information of the materials. Cathodoluminescence (CL) is the phenomenon which is the emission of light as the result of electron bombardment on materials. We can know that the bandgap structure (intrinsic bandgap energy or extrinsic energy states in the bandgap) of materials from the photon energy of the emitted light.

In this study, we developed a novel CL (light) detection system which compatible to an ordinary TEM. That is a light collectable TEM specimen stage. We carefully arrange the optical components such as mirror, lens and optical fiber within a TEM specimen stage. Lights reflected by the mirror are focused by optical lens located at the end surface of the mirror and transmitted to a spectrometer by optical fiber light guide. Therefore, we can easily conduct CL analysis with a standard TEM by just inserting the light collecting TEM specimen stage into the TEM. Moreover, we combined a specimen cooling system with the light collectable TEM specimen stage. As a specimen cool down, CL light emission intensity are increased and also we can get more detailed spectral information.

We investigated the emission characteristics of the microstructures in the GaN based light emitting devices by using the TEM-CL analysis system. First, we tried to understand optical properties of the dislocations in

GaN thin films. The most common substrate for GaN epitaxial growth, sapphire, is a very stable substrate in terms of its thermal, chemical, and mechanical properties. However, sapphire has the complex corumdum structure whereas III-nitride crystallizes in the wurzite structure. Furthermore, the lattice constants of sapphire and GaN are different. As a result, GaN epitaxial films have misfit dislocations that are typically on the order of 10^8-10^9 cm^{-2}. Monochromatic or panchromatic images show that the dislocations in GaN thin films act as non-radiative recombination center for band edge emission. Low-angle grain boundaries as arrangement of dislocations in GaN thin films also act as non-radiative sites for band edge emission.

Also, we studied about bandgap energy distribution of the InGaN QW active layers using the TEM-CL analysis system. It remains an unclearly explained fact that the radiative efficiency in III-nitrides, in particular InGaN/GaN blue emitters, exhibits low sensitivity to the presence of dislocations. In other words, high radiative efficiencies are obtained in InGaN/GaN blue emitters despite high dislocation densities. Many reports explains the origin of the defect insensitive light emission probability of the III-nitride material as the compositional alloy fluctuation, alloy clustering effects and phase separation effects that necessarily result in a variation of the bandgap energy and lead to local potential minima, where carriers are attracted to and could be confined to. The potential minima attract and

confine carriers and prevent them from diffusing toward the dislocation lines. Our TEM-CL system can acquire the full spectral information of each electron beam scanned region. So we can get the 2-dimensional “in-plane” emission property of the InGaN QW layers. In this study, therefore, we can show the microscopic evidences of the bandgap energy inhomogeneity of the InGaN QW structure by using the TEM-CL analysis system.

Finally, we show that the bandgap energy of the InGaN active layers is increased at the regions where dislocations penetrate the active layers from cross-sectional TEM observations and cathodoluminescence analysis. Therefore, dislocated regions in the InGaN active layers of the blue-light emitting diodes devices self-screen the carriers in the InGaN active layers. When the devices working, therefore, injected carriers in the InGaN active layers see the energy barriers at the dislocated region and consequently they will actively recombine at the other regions which have low bandgap energy.

Keywords**:** Cathodoluminescence, Transmission electron microscopy, Light emitting property, Dislocation, GaN, InGaN, Light emitting device, Bandgap energy

Student ID**:** 2006-20822

Sung-Dae Kim

Table of Contents

List of Figures

Figure 3.3.7. A schematic view of anti-localization of carriers at the region where penetrated by dislocations.

Chapter 1. Introduction

1. 1. Background

1. 1. 1. Cathodoluminescence

As accelerated electron beams interact with materials, various useful signals emitted which have structural, chemical and electrical information of the materials (Figure 1.1.1). Electron microscopy is a research field that uses these signals to understand and characterize properties of materials on a microscopic level. In an electron microscope, incident (primary) electrons may be scattered by the materials with little or no energy loss (elastic), or they will lose energy to excite the electronic state of the materials.

Cathodoluminescence (CL) is the phenomenon which is the emission of light as the result of electron bombardment on materials. In other words, some primary electrons will dissipate their energy with generating electron-hole pairs, which lead to the emission of photons in the ultraviolet, visible, and infrared range by radiative recombination. When the primary electrons transfer there kinetic energy to electrons in the materials, the electrons in valence band will be promoted into the conduction band. To make charge conservation, positively charged particles (holes) are generated in the valence band. These exited electrons and generated holes can move independently in each corresponding band structure. Occasionally, they recombine to make

charge neutrality with emission of light (radiative-recombination) or none (non radiative-recombination). The excited energy from the electron-hole pairs transferred to photon energy of the emitted light by radiative-recombination Therefore, we can know that the bandgap structure (intrinsic bandgap energy or extrinsic energy states in the bandgap) of materials from the photon energy of the emitted light. The energy between an initial state E_i and the final state E_f, or the wavelength, of the emitted photon can be found from the relation

$$h\upsilon = \frac{hc}{\lambda} = E_f - E_i \tag{1.1}$$

In many wide-bandgap materials, emission of photons occurs in the visible range (about 0.4 to 0.7 μm, corresponding to about 3.1 to 1.8 eV). In the literature, the luminescence results are presented in terms of both wavelength and energy. The wavelength λ (in μm) of a photon is related to the photon energy E (in eV) by $\lambda \approx 1.2398/E$.

There are a set of radiative transition modes between the conduction band, the valence band and other extrinsic energy state in the bandgap (Figure 1.1.2).

Mode 1 is and intraband transition: an electron excited well above the conduction-band edge dribbles down and reaches thermal equilibrium with the lattice. This thermalization process may lead to phonon-assisted photon emission or, more likely, phonon emission.

Mode 2 is an interband transition: this produces intrinsic luminescence. In this case, direct recombination between an electron in the conduction band and a hole in the valence band results in the emission of a photon energy $h\nu \approx E_g$. Although this recombination occurs from states close to the corresponding band edges, the thermal distribution of carriers in these states will lead, in general, to broad emission spectrum (near-band edge emission).

Mode 3 is the excitonic decay observable at low temperatures: both free excitons and excitons bound to and impurity may undergo such transitions. For bound excitons, one of the charge carriers is localized at a center that can assist in conserving momentum during the transition. This will be especially important in indirect-gap materials. In the literature, these transitions are often denoted with special symbols. Free-exciton recombination: X, recombination of an exciton bound at a neutral donor: D^oX, recombination of an exciton bound at a neutral acceptor: A^oX, recombination of excitons bound to the corresponding ionized impurities: D^+X and A^-X.

Mode 4, 5 and 6 arise from transition that start and/or finish on localized states of impurities in the gap. The recombination processes between free carriers and trapped carriers of the opposite type are known as the *Lambe-Klick model* (donor to free hole transition: D^oh) and *the Schon-Klasens model* (free electron to acceptor transition: eA^o) and the donor-acceptor pair (DAP) recombination model (model 6) is known as the *Prener-Williams*

model. These last three processes account for most of the processes in a wide variety of luminescent materials.

Recombination of electron-hole pairs may occur via non radiative-recombination processes such as multiple-phonon emission (direct conversion of the energy of an electron to heat), the Auger effect and recombination due to surface states and defects. Lattice defects can also introduce localized levels in the bandgap. Dislocations, for example, may produce both shallow levels due to the elastic strain fields and deep levels associated with dangling bonds. Native point defects such as vacancies and their complexes with impurity atoms may be resent and may introduce a wide range of localized levels in the bandgap.

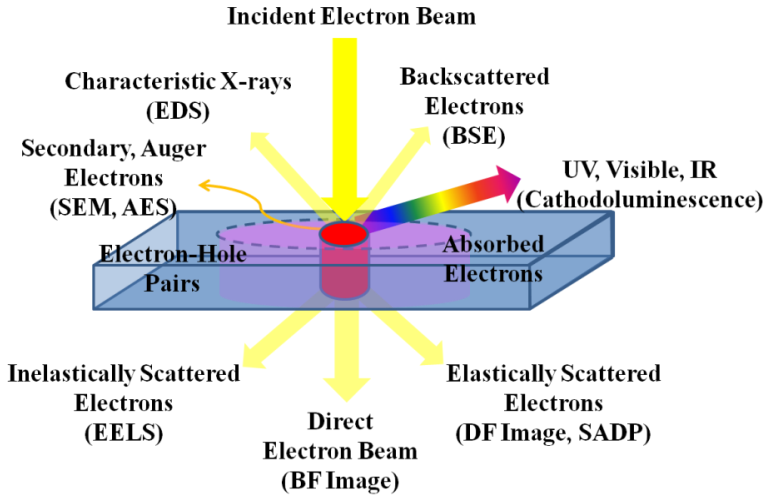

Figure 1.1.1. Various useful signals emitted by interaction between the electron beam and a sample.

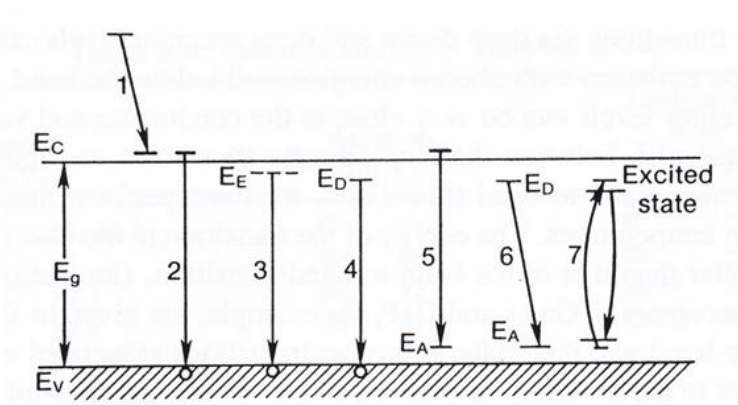

Figure 1.1.2. Schematic diagram of radiative transitions between the conduction band (E_C), the valence band (E_V) and excitons (E_E), donor (E_D) and acceptor (E_A) levels in a semiconductor.

1. 1. 2. Cathodoluminescence analysis techniques

Currently, there are two basic types of CL analysis systems. One is based on electron microscopes, scanning electron microscopes (SEMs), scanning transmission electron microscopes (STEMs), or TEMs equipped with CL detecting attachments. Using CL-SEM enables one to obtain CL images and display, for example, defect maps. There are significant differences between SEM and STEM-based systems and between these and systems attached to a TEM. By far most CL attachments are on SEM instruments because of the larger chambers and the ease of installing larger collection systems. The other approach employs a simple high-vacuum system containing an electron gun for the excitation of a material; no scanning capability is provided, so no image of a sample can be obtained; thus it is limited to spot mode CL only. The use of large-area, high power electron beams gives high CL intensity and thus make high-spectral-resolution analysis possible. In general, spatial and spectral resolutions vary inversely. In this type of CL analysis system, other optical measurements and/or processing of the sample are also possible. The main application of such systems is in depth-resolved CL studies.

The modes available in the SEM provide a variety of information about a sample. The secondary electrons are used for topographic information and voltage contrast, and the backscattered electrons provide atomic number contrast. Backscattered electrons can also be used for structural analyses of

solids (channeling patterns). X-rays provide information on the composition of the sample. The CL and charge collection (CC) modes are complementary techniques for the analysis of optical and electronic properties of semiconductors and insulators. In TEMs and STEMs, the transmitted and elastically scattered electrons provide microstructural information from images and crystallographic information from diffraction patterns. The inelastically scattered transmitted electrons provide information on composition using electron energy loss spectroscopy (EELS).

1. 1. 3. GaN-based light emitting diodes

The bandgap energy versus lattice constant of the III-nitride material system is shown in Figure 1.1.2. The III-nitride material system spans a very wide range of wavelength covering the deep UW, near UV, visible, and enven the near infrared spectral range. Of the three binary semiconductors InN, GaN, and AlN, epitaxially grown GaN has been shown to be synthesizable with the highest quality. It has generally been difficult to synthesize Al-rich AlGaN alloy and In-rich InGaN alloys with internal quantum efficiencies.

The energy-gap bowing can be expressed in terms of a constant, a linear term ($\propto x$) and a non-linear term [$\propto (1\text{-}x)$] according to

$$E_g^{AB} = E_g^A + \left(E_g^B - E_g^A\right)x + x(1-x)E_b \qquad (1.2)$$

With E_b called the *bowing energy* or *bowing parameter.* The bowing parameter is dependent on materials and strain condition.

The most common epitaxial growth direction of III-nitride is the *c*-plane of the hexagonal wurtzite structure. III-nitride grown on the *c*-plane has polarization charges located at each of the two surfaces of a layer. As a result of these charges, internal electric fields occur in III-nitrides that have a significant effect on the optical and electrical properties of this class of semiconductors. There are *spontaneous polarization* charges as well as strain-induced *piezoelectric polarization* charges (Figure 1.1.4). The direction of the internal electric field depends on the strain and the growth orientation.

The strain in the epitaxial layer can be compressive or tensile. In the compressive-strain case, the epitaxial layer of interest is laterally compressed. For example, InGaN is compressively strained when grown on a thick relaxed GaN buffer layer. In the tensile-strain case, the epitaxial layer of interest is expanded along the lateral direction. For example, AlGaN is under tensile strain when grown on a thick relaxed GaN buffer layer.

The quantum well layers have an internal electric field that spatially separates electrons and holes thereby preventing efficient radiative recombination. This is particularly true for thick quantum wells, e.g. > 10 nm. To avoid this deleterious effect, it is imperative that the quantum well layers are kept very thin. Quantum well thickness of 2-3nm are typically used to minimize such electron-hole separation effects.

The large electric fields caused by the polarization effects can be screened by a high free carrier concentration, which can be attained through either high doping of the active region or a high incurrent. Screening of the internal electric field also results in a blue-shift of the emission, frequently found in InGaN LED as the injection current is increased.

The most common substrate for GaN epitaxial growth, sapphire, is a very stable substrate in terms of its thermal, chemical, and mechanical properties. However, sapphire has the complex corumdum structure whereas III-nitride crystallizes in the wurzite structure. Furthermore, the lattice constants of sapphire and GaN are different. As a results, GaN epitaxial films

have misfit dislocations that are typically on the order of 10^8-10^9 cm^{-2}

Although a generally accepted explanation has not been established, it remains a fact that the radiative efficiency in III-nitrides, in particular InGaN/GaN blue emitters, exhibits low sensitivity to the presence of dislocations. That is, high radiative efficiencies are obtained in InGaN/GaN blue emitters despite high dislocation densities.

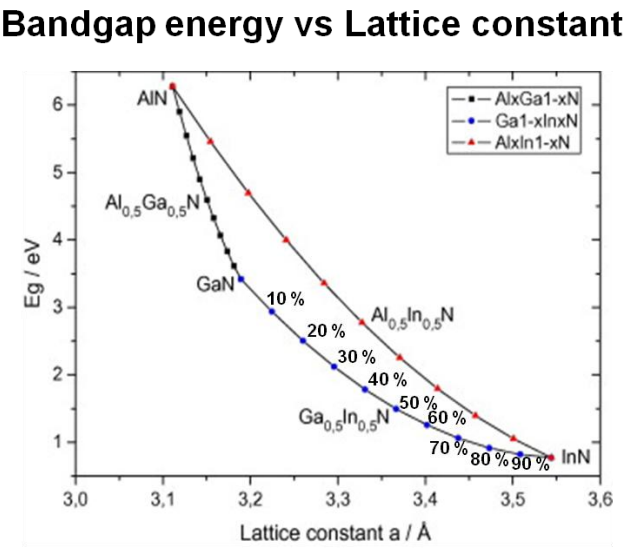

E.F.Schubert, Light-Emitting Diodes (Cambridge Univ. Press)

Figure 1.1.3. The bandgap energy versus lattice constant of the III-nitride material system.

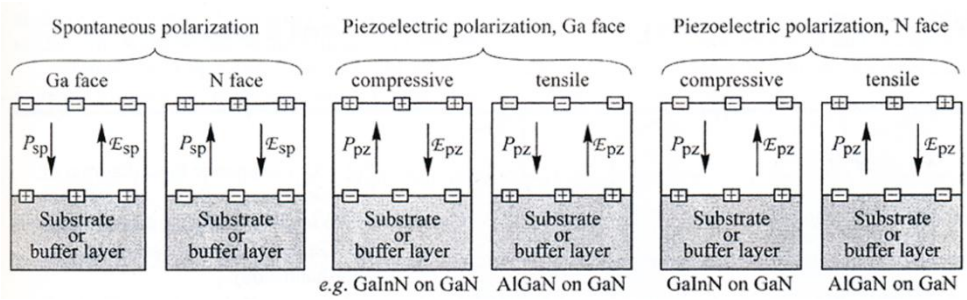

Figure 1.1.4. Surface charges and direction of electric field and polarization field for spontaneous and piezoelectric polarization in III-nitride materials for Ga and N face orientation.

1. 2. Scopes and organizations

This thesis consists of 4 chapters. Chapter 1 presented to the introduction as stated above.

Chapter 2 covers the Set-up of cathodoluminescence transmission electron microscopy. Chapter 2.1 presents the step-by-step manufacturing procedures of home-made light collectable TEM stage (combine with liquid nitrogen cooling system). In chapter 2.2, data processing of the CL spectral data which measured by CCD detector will be explained. Chapter 2.3 states the experimental details of the TEM-CL experiments.

Chapter 3 presents the TEM-CL study on the III-nitride based light emitting diodes. In chapter 3.1. optical properties of the threading dislocations in GaN films will be presented. Chapter 3.2 will show the Effective bandgap energy inhomogeneity of InGaN multiple-quantum wells (MQWs). And effects of the threading dislocations in GaN layer on the light emission property of the InGaN MQWs active layer will be discussed in Chapter 3.3.

At the conclusion, chapter 4 summarized this thesis.

Chapter 2. Set-up of cathodoluminescence transmission electron microscopy

2. 1. Development of light collectable specimen stage

2. 1. 1. Introduction

Cathodoluminescence analysis usually performed by using focused electron beam as excitation source. Electrons (negatively charged particles) can be focused by electromagnetic lenses to a spot which size of sub-nanometer range. By scanning the focused electron beam, therefore, we can collect CL spectra at each point of electron beam scanned region and also observe the microstructure of the region. Due to these advantages, most of the cathodoluminescence analyses have been conducted with scanning electron microscopes (SEM). In order to collect the emitted light from the sample, enough space in an electron microscope is needed to set up the light collecting optical components such as mirror, lens, light guide and etc. Therefore the scanning electron microscopes are good tools for cathodoluminescence because it has relatively large specimen chamber to arrange the optical components.

However, the scanning electron microscopes get only surface morphological information of the sample. Therefore, internal macrostructures such as dislocations, stacking fault or grain boundaries cannot be easily detected by the scanning electron microscopes. To overcome this

disadvantage of SEM, cathodoluminescence analyses with transmission electron microscopes (TEM) have been tried by few research groups. They could study about the optical properties of internal structures such as dislocations with cathodoluminescence analysis with a transmission electron microscope. They usually set up their own home-built cathodoluminescence detection system in a CL dedicated TEM. In other words, they attached a complicated light detection apparatus which has light align part, light collecting part and align part for TEM observation to the TEM column. These dedicated CL detection systems have some advantages such as fine alignment capability for light collecting and convenience to use or make its components. However, the focal length of the emitted light from sample to detector is too large to collect the emitted light effectively. Also, to set up independent detection system in a TEM column, some factors such as vacuum stability and mechanical stability should be carefully considered

In this study, we developed a novel CL (light) detection system which compatible to an ordinary TEM (Figure 2.1.1). That is a light collectable TEM specimen stage. We carefully arrange the optical components such as mirror, lens and optical fiber within a TEM specimen stage. To enlarge light collecting angle, we design a spherical parabolic mirror which covers specimen. Lights reflected by the mirror are focused by optical lens arranged at the end surface of the mirror and transmitted to a spectrometer by optical fiber light guide. From these design, we intended to minimize the loss

of emitted light during transmission. Also, we can easily conduct CL analysis with a standard TEM by just setting the light collecting TEM specimen stage on the TEM. Moreover, we combined a specimen cooling system with the light collectable TEM specimen stage. As a specimen cool down, CL light emission intensity are increased and also we can get more detailed spectral information.

2. 1. 2. Experimental detail

Figure 2.1.2 is a schematic of CL light collecting process by the light collecting TEM specimen stage. As electron beams illuminate a sample, CL signals (lights) are emitted to every direction. Direction of lights reflected by a parabolic surface in a mirror is parallelized to the direction of light focusing lens. And a biconvex lens focuses the parallel light to a focal point of the lens. Entrance surface of an optic fiber is located at the focal point of the lens to gather the focused light. Consequently, the lights are transmitted to a spectrometer by the optical fiber.

The parabolic mirror is an important component in the light collecting TEM stage. To make a parabolic surface, Al was used. Among the candidate materials, Al is the most suitable one because of its wide reflectance to visible light range. Figure 2.1.3 shows reflecting properties of the candidate materials for mirror. Considering the pole piece gap of the standard high resolution pole piece in a JEOL TEM, the thickness of the mirror was set below 3.5mm. The parabolic surface of the mirror was fabricated with a parabola equation. We set the focal length of the parabola as 0.5mm. At the focal length, a through hole was made to transmit the primary electron beam. At the focal point, lights are emitted by the interactions between the sample and the primary electron beams. And these lights are parallelized by parabolic surface of the mirror.

We used a 3mm diameter fused silica optical lens to focus the

parallelized lights. To increase the efficiency of the focusing light, a biconvex type lens was used. Although the parabolic surface of the mirror is carefully fabricate by the parabola equation, some aberrations may be made during machining process of the mirror. So, some of the reflected light has convergent direction to the focusing lens. By using the biconvex type lens, the convergent lights are also focused by the lens. Focal length of the lens is 6mm. We choose the focal length of the lens with considering of the critical acceptance angle for internal total reflection of the optical fiber light guide.

We used a high OH silisca-core optical fiber which is optimized to work in range from ultra-violet (UV) range to visible light (VIS) region. Core diameter of the optical fiber is 1000 μm to increase the intensity of the transmitted light. Buffering materials for silica coating is acrylate and Al coating layer was deposited on the optical fiber to protect the fiber core from the external mechanical shock. Also the Al coating layer protects the optical fiber from the thermal shock during liquid nitrogen cooling process. Optical fibers aer designed to transmit light from one end of the fiber to other with minimal loss of energy. The principle of operation in an optical fiber is total internal reflection According to Snell's Law, the new angle of the light ray can be predicted from the refractive indices of the two materials. At critical angle and below the critical angle, transmission is zero and reflection is 100%. The optical fiber used in this study has a numerical aperture (NA) of 0.22. If the fiber is in a vacuum or air, this translates into an acceptance angle θ_{max} of

12.7^{o} (full angle is ~25^{o}). When light is directed at the end of an optical fiber all the light rays or trajectories that are within $\pm 12.7^{o}$ cone are propagated down the length of the fiber by total internal reflection. Therefore, as we set the focal length of the focusing lens as 6mm, the optical fiber can make total internal reflection of the most of the focused by the lens.

We used a Ocean Optics QE65000 spectrometer. The spectrometer is a all-in-one type which has factory aligned optical bench and a CCD detector. We used this compact spectrometer to reduce loss of the lights by misalign of the optical bench. The optical bench of the spectrometer is aligned as symmetrical crossed Czerny-Turner type design. Focal length of the bench is 101.6mm and the entrance slit size is 200 μm. Groove density of the grating is 600 mm^{-1} and the blaze wavelength of the grating is 400nm. The groove density (lines/ mm^{-1}) of a grating determines its dispersion, while the angle of the groove determines the most efficient region of the spectrum. The greater the groove density, the better the optical resolution possible, but the more truncated the spectral range. And the blazed wavelength is the peak wavelength in an efficiency curve. For holographic gratings, it is the most efficient wavelength region. As using the grating which has a groove density of 600 mm^{-1} and the entrance slit size of 200 μm, the spectral resolution of the spectrometer is 3.13nm at 400nm. A Hamamatsu S7031-1006 CCD was used as light detector. It has 1024×58 pixels (pixel sized: 24 μm^{2}) and the pixel well depth is 300,000 electrons/well (1.5m elec/column). The sensitivity

of the CCD is 22electrons/counts and the quantum efficiency is 90% at the blazed wavelength (65% at 250nm)

A liquid nitrogen cooling system was also combined to the light collectable TEM stage (Figure 2.1.4). Liquid nitrogen dewar (200ml) was attached to the light collectable TEM stage holding part. And a oxygen free high purity Cu (OFHC) tube and related connector was assembled to the liquid nitrogen dewar. Through the inner hole of the Cu tube, the optical fiber was inserted. Fix the optical fiber on the Cu tube, we used a specially designed bolt. The bolt has a groove at the end surface to fix a ceramic ball. Using the bolt of 1mm diameter the optical fiber is fixed by the ceramic balls on the inner hole of the Cu tube. Therefore, the optical fiber is protected by thermal shock during cooling process and also thermal conduction through the optical fiber is reduced. The Cu tube fixed at the stage tip guide by Teflon block to reduce the thermal conduction through the TEM stage body. The early version (LN_2 cooling TEM-CL stage version 1) of the light collectable TEM stage (Figure 2.1.4) with liquid nitrogen cooling system has cu breaded wires which connect the Cu tube and specimen holding block. Through these Cu breaded wires heat was pumped out of the specimen. But the thermal connectivity of the Cu breaded wire is low and the thermal losses exist through the specimen holding block which fixed at the specimen stage tip guide. Therefore, we re-design the state tip guide and the specimen holding block. In the next version (LN_2 cooling TEM-CL stage version 2) of the light

collectable TEM stage (Figure 2.1.5), the specimen holding Cu block was directly assembled to the thermal conducting Cu tube. And the specimen holding cu block was fixed at the specimen tip guide with a point contact through the ceramic ball assembled bolt.

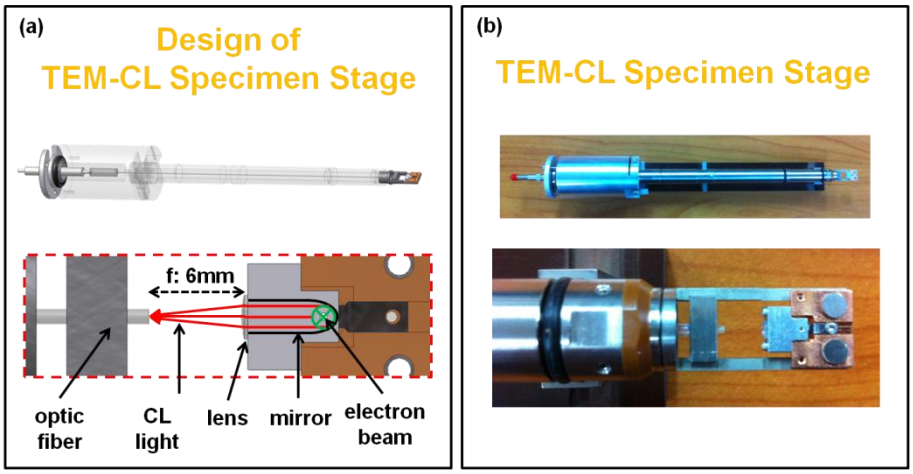

Figure. 2.1.1. (a) Design of the light collectable TEM stage and (b) Photo of the light collectable TEM stage prototype.

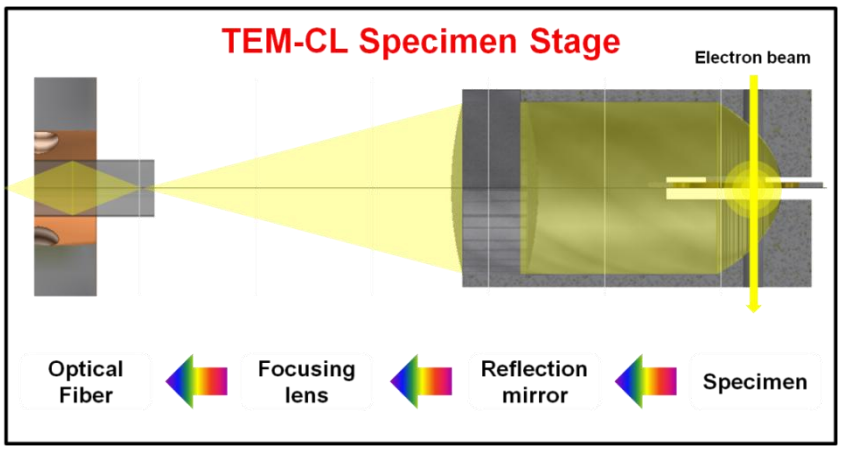

Figure 2.1.2. A schematic of CL light collecting process by the light collecting TEM specimen stage.

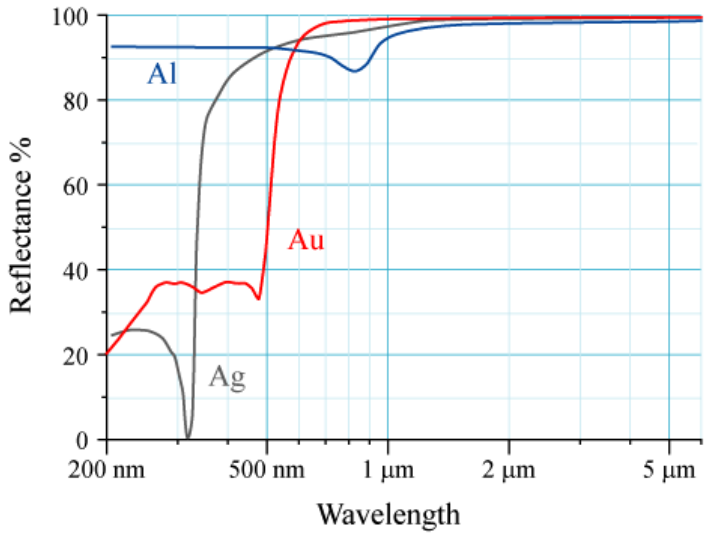

Figure 2.1.3. Reflectance of the candidate materials for parabolic mirror.

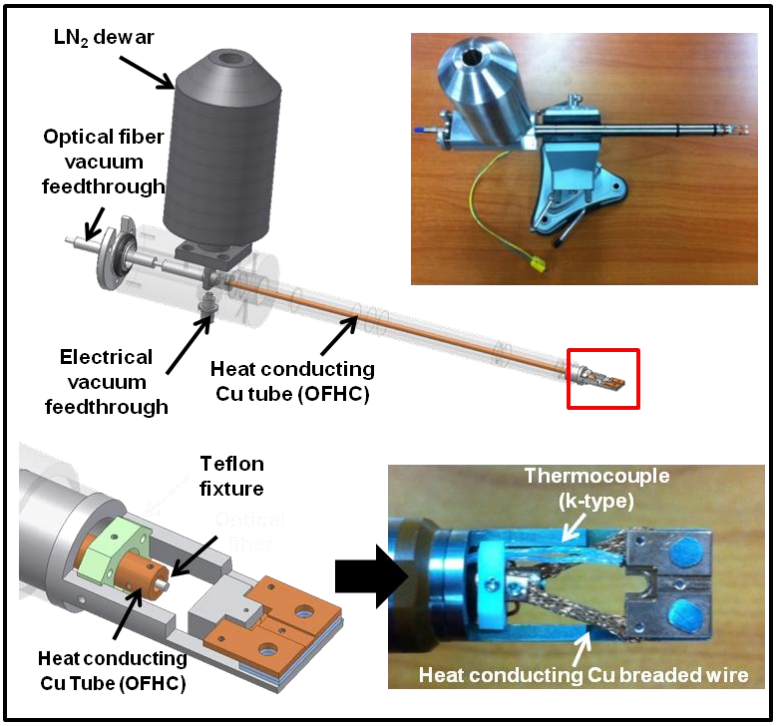

Figure 2.1.4. The light collectable TEM stage combined with the liquid nitrogen cooling system (version 1).

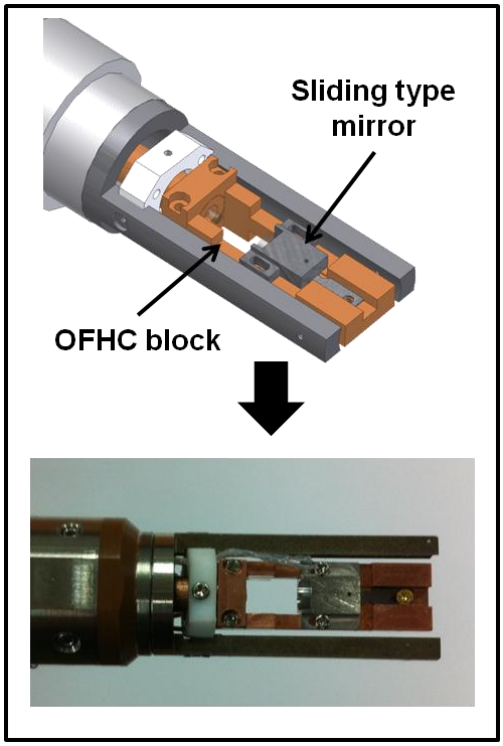

Figure 2.1.5. The light collectable TEM stage combined with the liquid nitrogen cooling system (version 2).

2. 1. 3. Results and discussions

The functionality of the light collatable TEM stage was tested by CL detection of ZnO nano-rods. Figure 2.1.6 shows a CL spectrum of the ZnO nano-rod. The CL spectrum has a near-band edge emission peak at 377nm and a broad 530nm wavelength centered emission band. Also from the Gaussian multiple peak fitting, the near band edge peak is decomposed with band edge peak and the donor-acceptor pair emission peak (390nm) at room temperature. From this experiment, we can conclude that the light collectable TEM stage can collect the CL signals from the specimen and the optical alignments are well optimized.

Also, the functionality of the liquid nitrogen cooling system (LN_2 cooling TEM-CL stage version 1) was tested in a modified SEM, which has a special port to accept the TEM holder (Figure 2.1.7) is the actual image of the SEM (JEOL, JSM 5200) with a test port. The temperature of the sample was measured by a K-type thermocouple which was mechanically attached on the sample holding Cu block. Actually, temperature of the sample was decreased and saturated at 150K after 40 min (Figure 2.1.8 (a)). Saturated temperature oscillated between $\pm$1K during 3hours with 200ml liquid nitrogen supplied.

We tried to decrease the saturated temperature of the liquid nitrogen cooling system by re-design the system. By some modifications of the cooling system design, newly designed light collectable TEM stage combined with the liquid nitrogen cooling system (LN_2 cooling TEM-CL stage version 2) cool down the

specimen to saturated temperature of 127K (Figure 2.1.8 (b)). The temperature of the specimen also saturated after 40min and the temperature oscillation is about ±1K.

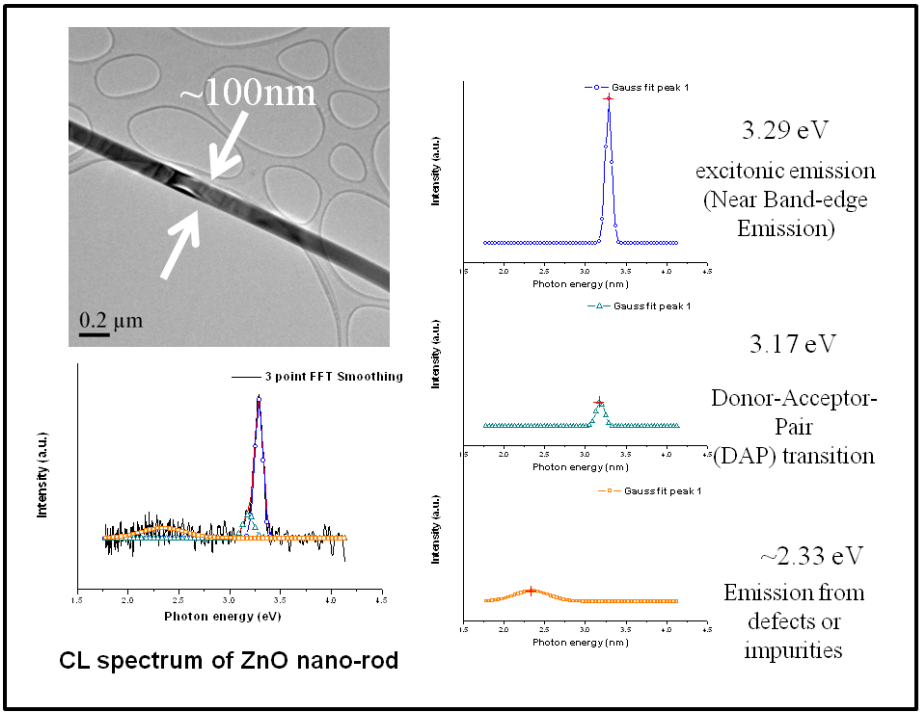

Figure 2.1.6. CL spectrum of the ZnO nano-rod.

Figure 2.1.7. A photo of the cooling test of the light collectable TEM stage combined with the liquid nitrogen cooling system in a SEM (JEOL, JSM 5200) with a test port.

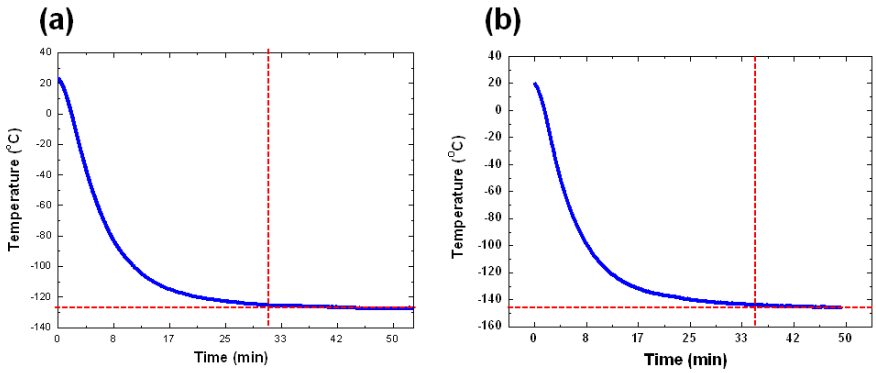

Figure 2.1.8. (a) Temperature of the sample cooled by the liquid nitrogen cooling system (version 1) (b) the liquid nitrogen cooling system (version 2).

2. 1. 4. Summary

In order to collect and detect the cathodoluminescence signals from the TEM sample, a novel light collectable TEM stage was developed. By optimized design and arrangement of optical components on the TEM stage, CL lights are successfully detected by a spectrometer. And to increase the CL intensity and get more detailed spectral information from the CL signals, we combined the liquid nitrogen cooling system to the light collectable TEM stage specimen. The sample can be cooled down to 127K with the cooling system.

2. 2. Data processing of collected CL spectra

2. 2. 1. Introduction

Detection of the cathodoluminescence is usually conducted by a photomultiplier tube (PMT) or a charge coupled device (CCD). Photomultipliers are constructed from a glass envelope with a high vacuum inside, which houses a photocathode, several dynodes, and an anode. Incident photons strike the photocathode material, which is present as a thin deposit on the entry window of the device, with electrons being produced as a consequence of the photoelectric effect. These electrons are directed by the focusing electrode toward the electron multiplier, where electrons are multiplied by the process of secondary emission. The electron multiplier consists of a number of electrodes called dynodes. Each dynode is held at a more positive voltage than the previous one. The electrons leave the photocathode, having the energy of the incoming photon (minus the work function of the photocathode). As the electrons move toward the first dynode, they are accelerated by the electric field and arrive with much greater energy. Upon striking the first dynode, more low energy electrons are emitted, and these electrons in turn are accelerated toward the second dynode. The geometry of the dynode chain is such that a cascade occurs with an ever-increasing number of electrons being produced at each stage. Finally, the electrons reach the anode, where the accumulation of charge results in a sharp current pulse indicating the arrival of a photon at the photocathode. A PMT

only measure the amplified electrical current at a specific wavelength in the spectrum. Therefore, we can get a full spectrum at a specific region by rotating the grating in a spectrometer which takes a few minutes. Or we just get the intensities of a fixed wavelength by fix the grating of a spectrometer and scanning the electron beam. So, we should choose get just a spectrum at a point or an intensity map of a fixed wavelength by using a PMT.

On the contrary to the PMTs, using charge coupled devices we can store spectra from every point where electron beam scans. In other words, lights are dispersed by a grating of a spectrometer to give a spectrum and these dispersed elements of the lights are independently detected by an each pixel of a CCD array. So, we can get every spectra of electron beam scanned region. If we could get this full spectral information of the sample, we can conduct various type of data processing.

2. 2. 2. Experimental detail and Results

Figure 2.2.1 shows the schematic of CL signal detection experiment. We use an electron beam scanning unit of Oxford company which is Semi-STEM. The unit controls the electrical current of the condenser lens deflection coil of TEM. Through this electron beam control unit, we can set the size of electron beam scanned region and rate of electron beam scan. Also, we set the acquisition parameters of detector with same value of electron beam scanning. Therefore, electron beam scanning and the spectrum detection are synchronized. Consequently, we can store every spectra of electron beam scanned region. Also, by using the TEM micrographs, we can match the microstructure of the sample with the spectral information.

By using this 2-dimenstional CL spectral information, we can analyze the optical properties of microstructure in a sample by various data processing methods. We can make a monochromatic spectral image by select intensity value of specific CCD pixel or a panchromatic image by sum the intensity values of selected pixels (Figure 2.2.2 (a)). Analysis of spectrum which measured by PMTs, just one spectral image could be made by one scanning of electron beams. On the contrary to PMTs, we can make monochromatic images of every wavelength range by just select different pixel of CCDs.

Also, we can make a hyper-spectral image of the CL spectra (Figure 2.2.2 (b)). The hyper-spectral image is three dimensional view of the spectra.

Wavelength, x-coordination of scanned line and photon counts are the axial components of the image. From the hyper-spectral image, we can analyze the shift of the spectrum in an arbitrary scanned line.

Wavelength map of the CL spectra can be made by using the stored spectral information. Taking the fast Fourier transformations of every stored spectrum, wavelengths of a specific peak are measured. Consequently, we can make a map of peak wavelength distribution of spectra (Figure 2.2.2 (c)). Converting the peak wavelength distribution map to photon energy distribution by wavelength-photon energy equation, we can also make a energy distribution map of the spectra. As photon energy of the peak wavelength of a CL spectrum is same with the band-gap energy of the scanned region, we could make a 2-dimensitonal band-gap energy distribution plot (Figure 2.2.2 (c)).

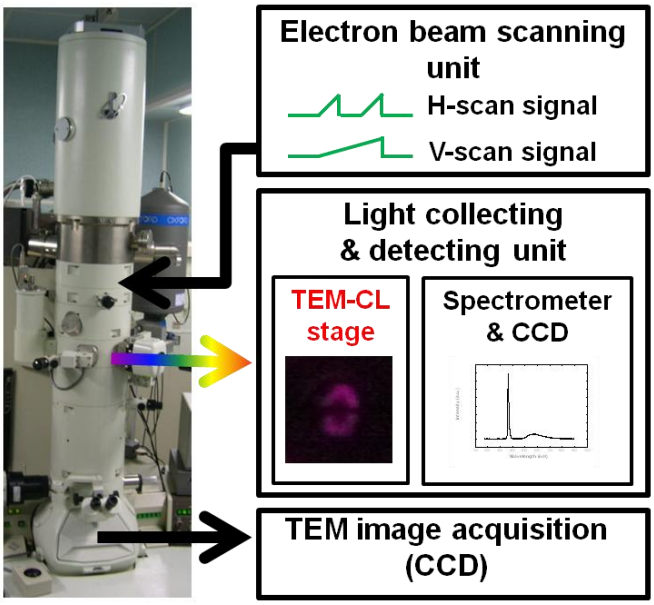

Figure 2.2.1. A schematic of the CL signal detection in a transmission electron microscope.

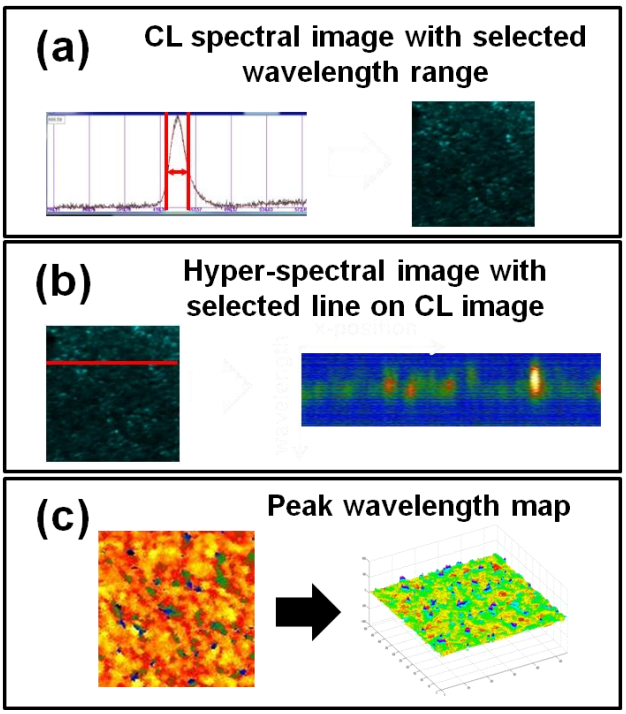

Figure 2.2.2. CL data processing using the full spectral information.

2. 2. 3. Summary

We store every CL spectra of the electron beam scanned region by using a CCD detector. The stored 2-dimensional full spectral information was used to elucidate the optical properties of the microstructure in a TEM sample by various data process methods. We can make conventional monochromatic, panchromatic CL image, hyper-spectral CL image and the peak wavelength map of a sample. And also we can analyze the 2-dimensional band-gap structure of the sample by the band-gap energy plot.

2. 3. TEM-CL experimental detail

The TEM-CL experiments was conducted in a JEOL 2010F TEM. Acceleration voltage of electron beam was set as 120 kV to reduce the defect generation during electron beam scanning. Current density of the electron beam was 50pA/cm^2. The TEM sample was cooled down to 127K before the CL measurement. Oscillation of the saturated temperature is about ±1K.

Electron beam scanning was conducted by the Semi-STEM control unit of Oxford Company. We measured the CL spectra from 138×128 points which size is depends on magnifications. Illumination time of each point was set as 200 msec.

CL spectral was detected by a CCD attached to a spectrometer of Ocean Optics QE65000 model. The spectrometer has a gratin of 600/mm groove density and the entrance slit size of 200 μm. The CCD arrays were cool down to -20 ^oC by thermo-electric cooler during CL measurement. Acquisition time of each measurement was 200 msec.

TEM specimen was prepared by mechanical polishing followed by Ar^+ ion milling (PIPS, Gatan). To reduce defect formation during the ion milling process, we tried to reduce the ion milling time below 60 min.

Annular dark field (ADF) STEM images and weak beam dark field images were taken at the same region of the CL spectra measured by Tecnai F20 TEM after CL measurement.

Chapter 3. TEM-CL analysis of GaN-based light emitting devices

3. 1. TEM-CL analysis of threading dislocations in GaN thin films

3. 1. 1. Introduction

The most common substrate for GaN epitaxial growth, sapphire, is a very stable substrate in terms of its thermal, chemical, and mechanical properties. However, sapphire has the complex corumdum structure whereas III-nitride crystallizes in the wurzite structure. Furthermore, the lattice constants of sapphire and GaN are different. As a result, GaN epitaxial films have misfit dislocations that are typically on the order of 10^{8}-10^{9} cm^{-2}. Generally, dislocation lines are electrically charged so that the region surrounding a dislocation line is either coulombically attractive or repulsive to a free carrier. The nature of the coulombic interaction (attractive or repulsive) depends on the polarity of the dislocation line and the polarity of the carrier. Initially, electrons are attracted but holes are repelled due to the potential created by the dislocation. However, the continued collection of electrons will screen the dislocation potential thereby reducing the repulsive barrier for holes. As a result, electrons and holes will recombine non-radiatively via

electron states of the dislocation line. Understanding the electronic properties of such dislocations in GaN films is currently a subject of much interest. The luminescent properties are important for the operation of light emitting devices. Band-to-band luminescence is observed at room temperature in high quality GaN films. Yellow luminescence has been observed in undoped and silicon-doped thin films. The origin of the yellow luminescence band is still unknown. Two models have been suggested to explain the recombination mechanism. Ogino et al. proposed that the yellow emission is due to a transition from a shallow donor to a deep acceptor level at $E \approx Ev+0.86$eV. Recently, Glaser et al. concluded from optically detected magnetic resonance experiments that the yellow transition involves a deep donor at $E \approx Ec-1.0$eV and, therefore, a shallow acceptor at $Ev+0.2$eV.

In this study, we investigated the emission characteristics of the dislocations in the GaN based light emitting devices by using the TEM-CL analysis system.

3. 1. 2. Experimental detail

Our TEM-CL system is composed of the light collecting and the light detection part. We developed a novel TEM specimen stage (TEM-CL stage) as the light collecting part. Optical components such as mirror, lens and optic fiber are arranged in a standard specimen stage of JEOL TEM so that it could maximize the collection of the emitted light from a sample.

A liquid nitrogen cooling finger was embedded into the TEM-CL stage, which can maintains the temperature of the sample at 150K to improve CL emission efficiency and reduce the carrier recombination diffusion length. Through an optical fiber, the collected light was transmitted to the light detection part which has a spectrometer and a charge-coupled device (CCD). We used an all-in-one spectrometer of Ocean Optics QE56000 model equipped with a CCD located at the end of the optical bench. With a grating of 600 mm^{-1} groove density and a fixed entrance slit (size: 200μm), the spectral resolution of the spectrometer is 3.13nm at 400nm.

TEM-CL experiments are performed with a JEOL 2010F TEM at 120keV accelerating voltage and the electron current density of 50pA/cm^2. To acquire 2-dimenstional data sets of the CL spectra, the focused electron beam was scanned onto the area of interest using an external scanning unit of Oxford instrument (SEMI-STEM).

TEM samples of InGaN QW were prepared by mechanical polishing followed by ion milling of 3.5 kV Ar^+ ions (Gatan PIPS). Weak beam dark

field (WBDF) images and STEM images were taken by a Tecnai F20 TEM from the same area of CL spectra measured.

GaN samples were prepared by conventional low pressure metal-organic chemical vapor deposition (MOCVD) method. The sample consists of a 3 μm-thick GaN layer grown on (0001) sapphire substrate. Trimethylgallium (TMGaand ammonia (NH_3) were used as Ga, In and N sources and hydrogen as carrier gas. Growth temperature of the GaN layer is 1040 ^{o}C.

3. 1. 3. Results and discussions

Figure 3.1.1 is a room temperature CL spectrum of a GaN thin film. There are two main peaks in the CL spectrum which are band edge emission at 364nm and broad yellow band emission from 500 to 650nm, respectively. The band edge emission originated from the band-to-band transition of the exited electrons. And the yellow band emission comes from defect states within the bandgap. The origin of the yellow band emission is still remained unclear.

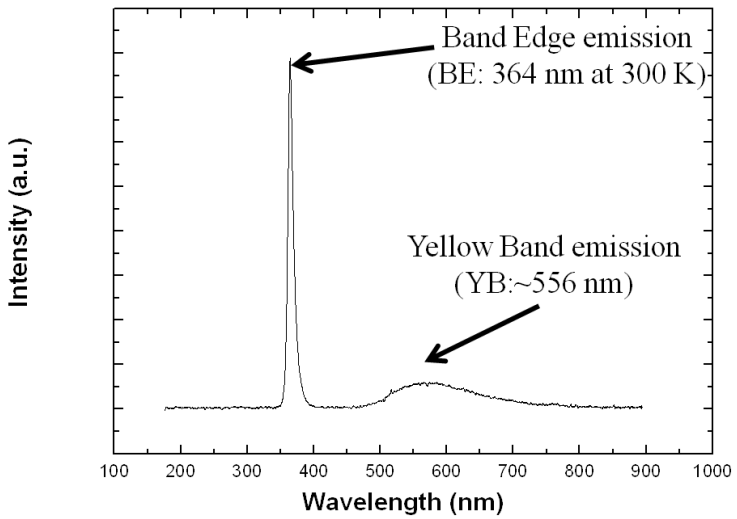

Figure 3.1.1. Room temperature CL spectrum of a GaN thin film.

We took a monochromatic image of a GaN film. Figure 3.1.2 (a) is a plan-view TEM image of the sample and a monochromatic CL spectral image (Figure 3.1.2 (b)) were taken at the region with red square. These figure shows that threading dislocations in the GaN film is shown as dark spots in the CL spectral image. So, we can easily know that the threading dislocations act as non-radiative recombination center for band edge emission of GaN. One thing to note is that there is a grain-like contrast in the CL image. With figure 3.1.3, we can know that the grain-like contrast in the CL image is come from the arrangement of the dislocation that is low-angle grain boundaries. The low temperature GaN buffer layer usually is deposited before the high temperature GaN growth to reduce the threading dislocation density. The low-angle grain boundaries are originated from the low temperature GaN buffer layer. As the threading dislocations act as non-radiative recombination center, the low-angle grain boundaries which are arrangements of dislocations also affect the band edge emission property of GaN films.

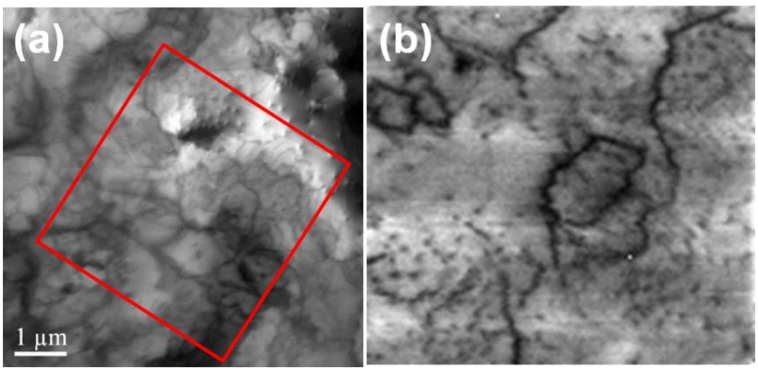

Figure 3.1.2. (a) Plan-view TEM image of the sample and (b) monochromatic image of band edge emission of a GaN film.

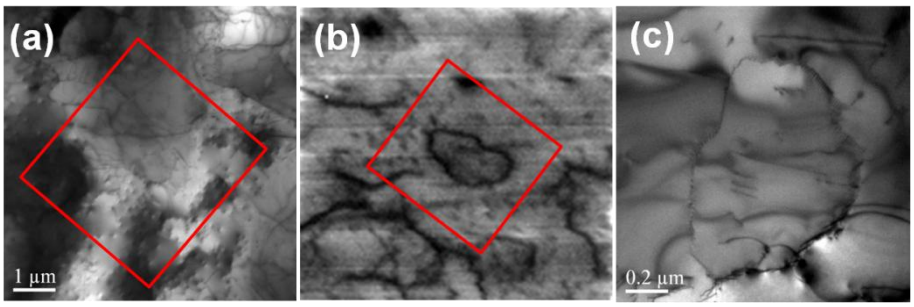

Figure 3.1.3. (a) Plan-view TEM image of the sample, (b) monochromatic image of band edge emission of a GaN film and (c) high magnification plan-view TEM image at the squared region of (b).

3. 1. 4. Summary

We investigated the emission characteristics of the microstructures in the GaN based light emitting devices by using the TEM-CL analysis system. First, we tried to understand optical properties of the dislocations in GaN thin films. The most common substrate for GaN epitaxial growth, sapphire, is a very stable substrate in terms of its thermal, chemical, and mechanical properties. However, sapphire has the complex corumdum structure whereas III-nitride crystallizes in the wurzite structure. Furthermore, the lattice constants of sapphire and GaN are different. As a result, GaN epitaxial films have misfit dislocations that are typically on the order of 10^{8}-10^{9} cm^{-2}. Monochromatic or panchromatic images show that the dislocations in GaN thin films act as non-radiative recombination center for band edge emission. Low-angle grain boundaries as arrangement of dislocations in GaN thin films also act as non-radiative sites for band edge emission. Furthermore, we investigated about the yellow band emission in the CL spectrum of GaN films. According to panchromatic images, we can know that tendencies of the yellow band emission at the dislocated region in GaN films are changed by doping process. As a result, we can know that the yellow band emission is not originated from the dislocations

3. 2. Effective bandgap energy inhomogeneity of InGaN multiple-quantum wells (MQWs)

3. 2. 1. Introduction

Group III nitrides semiconductors have been the most promising materials to fabricate short-wavelength light-emitting diodes (LEDs) for full-color display and laser diodes (LDs) for high-density optical storage and high resolution printing. Bandgap energy of the group III nitrides, comprising the (Al-In-Ga)N alloys, is in the range from 0.65eV to 6.04eV depends on the concentrations of group III metal elements. Therefore, wavelength of the emitted light from these materials could be controlled from infrared to ultraviolet region by adjusting the composition of the group III element in the (Al-In-Ga)N alloys.

After the introduction by Shuji Nakamura et al, the InGaN alloys have been commonly used as an active layer of blue-UV LEDs and LDs. Most surprising fact was that these In-containg III nitride light emitting devices exhibit high emission efficiency despite its high density of lattice defects such as dislocations. In other words, due to the lattice mismatches between the group III nitride semiconductors and the non-native substrate such as c-plane (0001) sapphire, the III nitride based LEDs and LDs have much high defects density compared with the LEDs and LDs fabricated using conventional III-V compound semiconductors (AlGaAs and AlInGaP).

Therefore, there have been numerous reports to explain the origin of

the defect-insensitive emission characteristics of the InGaN active layer. Most of them proposed the origin of such ‘defect-insensitivity’ is the localization of excitons at certain potential minima originated from the effective bandgap energy inhomogeneity of InGaN layer. Chichibu et al. studied the emission mechanism of InGaN quantum well (QW) structures using numerous luminescence analysis techniques such as electroluminescence (EL), static/time-resolved (TR) photoluminescence (PL), cathodoluminescence (CL) and positron annihilation measurements. From systematic analysis of the emission properties of InGaN QW structure, they explain the origin of the defect-insensitive nature of the emission probability of InGaN QW as the existence of localized radiative centres that capture the excitons and prohibit the recombination of excitons at the non-radiative centres. Subsequently, to show the microscopic evidences of the localized radiative centres in InGaN QW structure, many research groups suggested the presence of the In-rich InGaN quantum dots (QDs) through transmission electron microscopy (TEM) analysis. However, the formation of such In-rich QD may depends on the growth conditions and there have been arguments about the possibility to observe the high-energy (above 200keV acceleration voltage) electron beam induced damages as the existence of QDs.

Cathodoluminescence studies of InGaN QW structure also conducted by some researchers due to its superior spatial resolution compared with the PL or EL analysis and ability to directly correlate the luminescence properties

with the microstructure. However, most of the cathodoluminescence studies were performed with scanning electron microscopes (SEM-CL). Although the SEM-CL analysis could show the luminescence properties at a specific region by scanning the focused electron beam, SEM provides just microscopic information of the surface morphology. Therefore, effects of the internal defects such as dislocations in the LEDs and LDs on the luminescence property of active layers cannot be clearly known by just SEM-CL analysis. To overcome this disadvantage of SEM-CL analysis, CL studies of III nitride based light emitting devices have been carried out with transmission electron microscopes (TEM-CL) by few research groups. They showed that the threading dislocations (TDs) in GaN films are the non-radiative recombination centres by matching the CL image with TEM micrographs. However, they could not show the microscopic evidences of the localized radiative recombination centers in the InGaN active layers.

In this study, we investigated the emission characteristics of the InGaN QW active layers using an improved home-built TEM-CL system. Our TEM-CL system can acquire the full spectral information of each electron beam scanned region. So we can get the 2-dimensional “in-plane” emission property of the InGaN QW layers. Consequently, we can show the microscopic evidences of the bandgap energy inhomogeneity of the InGaN QW structure.

3. 2. 2. Experimental and analysis detail

Our TEM-CL system is composed of the light collecting and the light detection part. We developed a novel TEM specimen stage (TEM-CL stage) as the light collecting part. Optical components such as mirror, lens and optic fiber are arranged in a standard specimen stage of JEOL TEM so that it could maximize the collection of the emitted light from a sample.

A liquid nitrogen cooling finger was embedded into the TEM-CL stage, which can maintains the temperature of the sample at 150K to improve CL emission efficiency and reduce the carrier recombination diffusion length. Through an optical fiber, the collected light was transmitted to the light detection part which has a spectrometer and a charge-coupled device (CCD). We used an all-in-one spectrometer of Ocean Optics QE56000 model equipped with a CCD located at the end of the optical bench. With a grating of 600 mm^{-1} groove density and a fixed entrance slit (size: 200μm), the spectral resolution of the spectrometer is 3.13nm at 400nm.

TEM-CL experiments are performed with a JEOL 2010F TEM at 120keV accelerating voltage and the electron current density of 50pA/cm^2. To acquire 2-dimenstional data sets of the CL spectra, the focused electron beam was scanned onto the area of interest using an external scanning unit of Oxford instrument (SEMI-STEM).

TEM samples of InGaN QW were prepared by mechanical polishing followed by ion milling of 3.5 kV Ar^+ ions (Gatan PIPS). Weak beam dark

field (WBDF) images and STEM images were taken by a Tecnai F20 TEM from the same area of CL spectra measured.

InGaN/GaN QW samples were prepared by conventional low pressure metal-organic chemical vapor deposition (MOCVD) method. The sample consists of a 3 μm-thick GaN layer grown on (0001) sapphire substrate and three period InGaN (3nm)/GaN (20nm) multiple quantum wells (MQWs) capped with a 150 nm-thick GaN layer. Trimethylgallium (TMGa), trimethylindium (TMIn) and ammonia (NH_3) were used as Ga, In and N sources and hydrogen as carrier gas. Growth temperature of the InGaN and GaN layer is 740 ^oC and 1040 ^oC, respectively.

3. 2. 3. Results and discussions

Figure 3.2.1 is a plan-view bright field (BF) TEM image of a InGaN/GaN multiple-quantum well structure. There are threading dislocations which density is about ~10^8/cm^2. In a plan-view TEM image, the InGaN quantum well active layers cannot be clearly distinguished because thickness of the InGaN layers (6~7 nm) is much narrow compared with the total thickness of the plan-view sample (~200 nm). However, a CL spectrum shows band edge peak of the InGaN active layers (Figure 3.2.2). The spectrum was taken by illuminating the sample by electron probe which diameter is about 1μm. The CL spectrum also shows band edge emission peak (~360 nm) of GaN substrate and broad yellow band emission (520~600 nm) from defects state in the GaN layer. Intensity of the InGaN layers band edge peak is much higher than the band edge emission peak of GaN. It is maybe due to the carrier confinement in the InGaN quantum wells. Optical properties of the InGaN active layers were investigated by using this band edge emission. We took the CL spectra of the sample with scanning electron beams normal to the InGaN active layers.

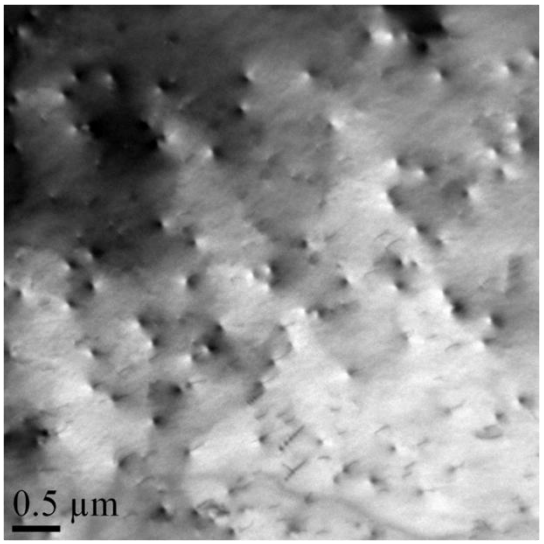

Figure 3.2.1. Plan-view bright field (BF) TEM image of a InGaN/GaN multiple-quantum well structure.

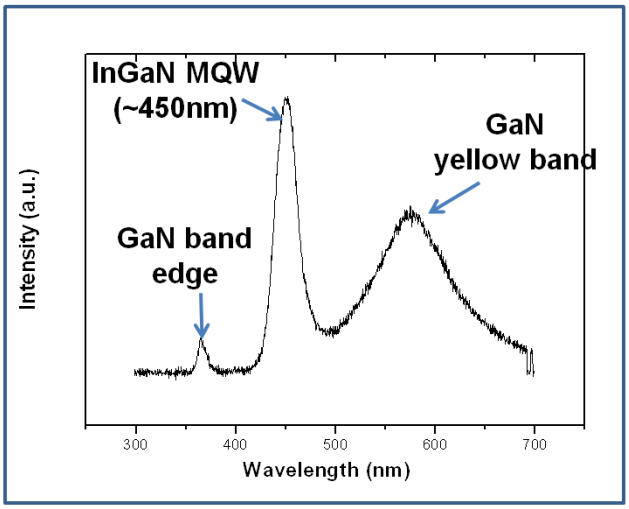

Figure 3.2.2. CL spectrum of the InGaN/GaN multiple-quantum well structure.

Figure 3.2.3 (a) and (b) show the panchromatic CL spectral image obtained at room temperature including the 400-460 nm light emission from plan-view of the InGaN sample and a bright field (BF) image of the CL signal measured region, respectively. Figure 3.2.3 (a) reveals bright spots with ~120 nm in diameter, which indirectly tells us that the un-even distribution of the radiative recombination centers excited by electron beam.

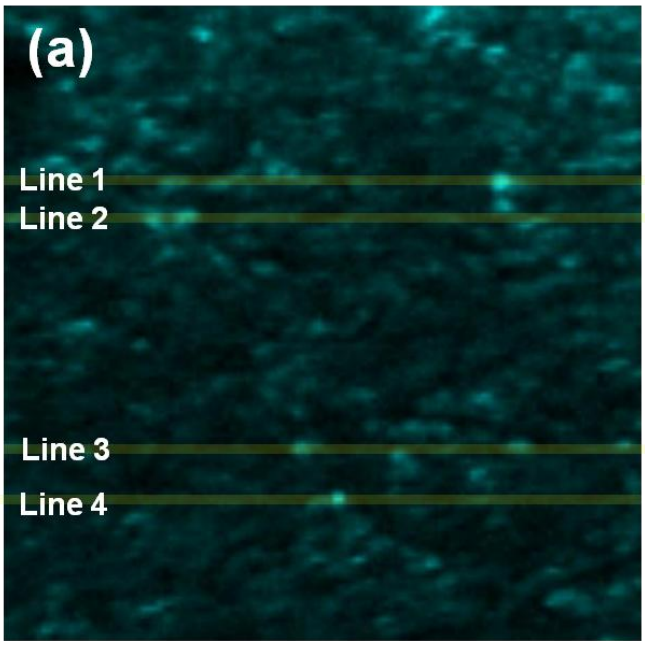

Figure 3.2.3 (a) Panchromatic CL spectral image obtained at room temperature including the 400-460 nm light emission from plan-view of the InGaN sample.

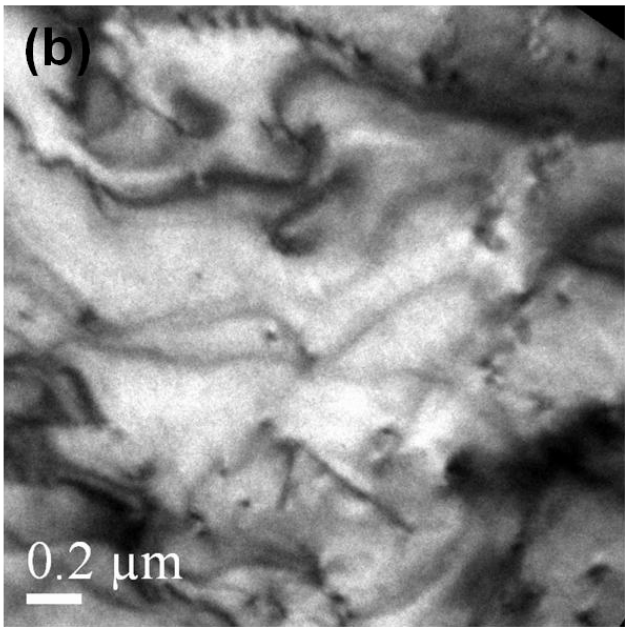

Figure 3.2.3 (b). bright field (BF) image of the CL signal measured region.

Peak wavelength shifts in the bright spots were investigated from 4 line scans to see the local variations in the light emission. Figure 3.2.4 reveals hyper-spectral image with position from the 4 line scan shown in Figure 3.2.3 (a). The hyper-spectral image is an arrangement of spectra through the x-coordination where the spectrum was obtained. From the hyper-spectral image, we could know that peak wavelength of the bright spot region is fluctuated (± 5nm) around centered at 450 nm. According to the *Vegard's Law*, the peak wavelength of emitted light is related to the In concentration. Therefore, the fluctuations of the peak wavelength in the Figure 3.2.4 shows that In concentration in most of the bright spots is not uniform. It was suggested by researchers that In-rich region (either quantum dos or disk) formed localized small band gap region to enhance the recombination probability by localization of carriers. So, the enhanced radiative recombination probability of bright spots in the Figure 3.2.4 might be originated from the In concentration non-uniformity in that region. In order to clarify the non-uniformity of the In concentration in the InGaN layer, “in-plane” wavelength map was investigated.

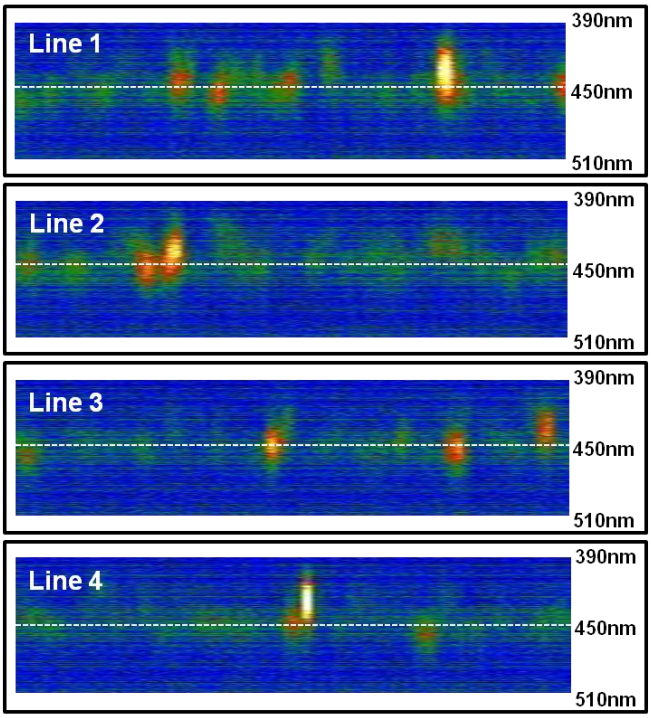

Figure 3.2.4. Wavelength map with position from the 4 line scan shown in Figure 1(a).

Figure 3.2.5 shows the two dimensional distribution of the peak wavelengths to confirm the non-uniformity of In concentration. Most of the regions shows 450 nm (orange color) or longer wavelength (455 nm, yellow color) that means most of the region have In concentration of 17% (orange color region) or 18% (yellow region) according to the *Vegard's Law*. Therefore the Figure 3.2.5 shows the microstructural evidences of the existence of the In-rich regions in the InGaN layers. One thing should be noted that is some of the localized regions shows emission of 440nm (green color) or 430nm (blue color). It will be discussed at the chaper 3.3.

Figure 3.2.6 shows the distribution of the bandgap converted from the wavelength variations using the wavelength and photon energy relationship, which distinctly reveals the bandgap fluctuation reported by many. Most of the region shows bandgap of 2.8 eV (green color), but some with pitfalls (red color) with 0.1 eV smaller than surroundings. This mapping directly reveals that the localized carrier trapping sites proposed by many researchers.

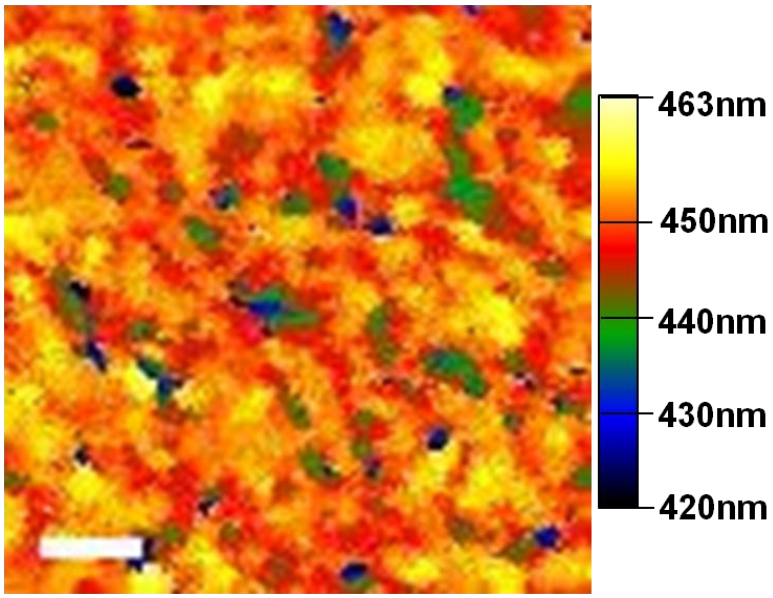

Figure 3.2.5. Two dimensional distribution of the peak wavelengths to confirm the non-uniformity of bandgap energy. Scale maker has length of 400nm.

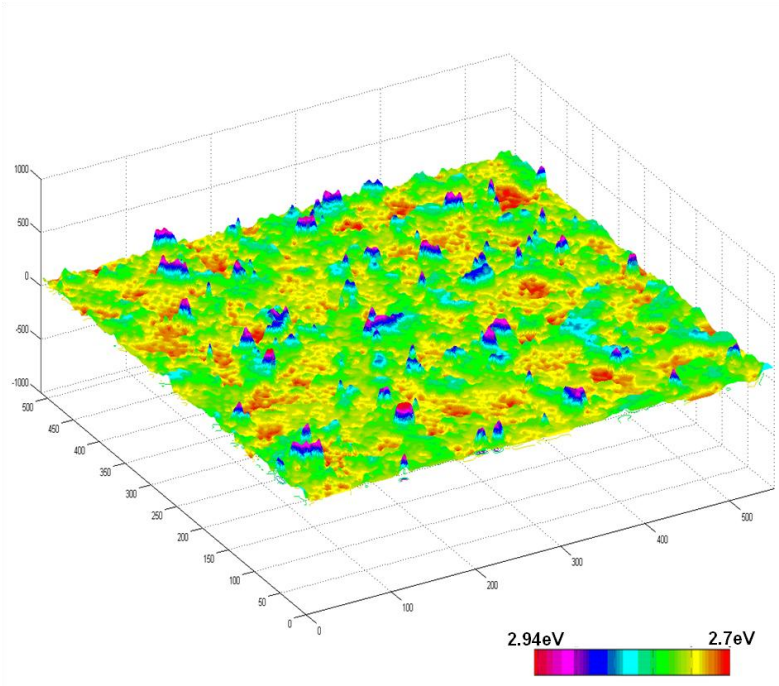

Figure 3.2.6. Distribution of the bandgap converted from the wavelength variations using the wavelength and photon energy relationship.

3. 2. 4. Summary

In this study, we have investigated cathodoluminescence emission of the InGaN multiple-quantum wells active layers for blue-light emitting diodes. The non-uniform radiative recombination probability of the carriers in the InGaN active layers is shown by the panchromatic spectral image of the InGaN layers. This non-uniform distribution of the light emission is come from the non-uniformity of In concentration in the InGaN active layers. In other words, the band edge peak wavelength of the InGaN layers is fluctuated around 450nm. The “in-plane” wavelength map of band edge emission peak of InGaN layers also shows the inhomogeneity of the In concentration. From the band-gap energy plot, we can know that the carriers maybe concentrated at the hump regions in the band-gap energy plot. So, the probability of the radiative recombination is increased at that region. In this study, therefore, we could show the microstructural evidences of the carrier localization.

3. 3. Effects of the threading dislocations in GaN layer on the light emission property of the InGaN MQWs active layer

3. 3. 1. Introduction

The most common substrate for GaN epitaxial growth, sapphire, is a very stable substrate in terms of its thermal, chemical, and mechanical properties. However, sapphire has the complex corumdum structure whereas III-nitrides crystallized in the wurzite structure. Furthermore, the lattice constants of sapphire and GaN are different. As a result, GaN epitaxial films have misfit dislocations that are typically on the order of 10^8-$10^9 cm^2$.

It remains a fact that the radiative efficiency in III-nitrides, in particular InGaN/GaN blue emitters, exhibits low sensitivity to the presence of dislocations. That is, high radiative efficiencies are obtained in InGaN/GaN blue emitters despite high dislocation densities. This is illustrated Figure 3.3.1 which compares the normalized efficiency of different semiconductors as a function of the dislocation density in GaAs, AlGaAs, GaP, and GaAsP.

Many reports explains the origin of the defect insensitive light emission probability of the III-nitride material as the compositional alloy fluctuation, alloy clustering effects and phase separation effects that necessarily result in a variation of the bandgap energy and lead to local potential minima, which carriers are attracted to and could be confined to. This explanation would be particularly suitable for ternary and quaternary alloy semiconductors such as InGaN and AlInGaN. The potential minima

attract and confine carriers and prevent them from diffusing toward the dislocation lines. However, they could not show any microstructural evidences of the localized potential minima. And the explanation cannot gives the role of the dislocations to the bandgap structure of the InGaN, AlInGaN alloy.

Hangler *et al.* pointed out that a reduction of InGaN/GaN quantum well thickness occurs in the vicinity of V-shaped defects of III-nitride epitaxial layers. The authors proposed that the higher bandgap energy associated with the thinner InGaN quantum wells shields the dislocation line-defect from mobile carriers located in the thicker InGaN quantum wells. As a result, a high radiative efficiency would be maintained in quantum well structures despite the presence of dislocations. However, they could not show direct correlation between the thinner InGaN quantum wells region and increased bandgap energy.

In this study, we will show the effects of the threading dislocations in the InGaN/GaN structure on the light emission properties of the InGaN active layers.

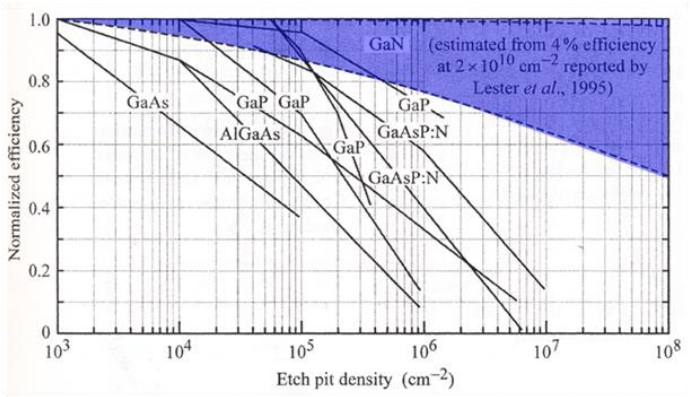

E.F.Schubert, Light-Emitting Diodes (Cambridge Univ. Press)

Figure 3.3.1. Dependence of radiative efficiency on etch pit density.

3. 3. 2. Experimental and analysis detail

Our TEM-CL system is composed of the light collecting and the light detection part. We developed a novel TEM specimen stage (TEM-CL stage) as the light collecting part. Optical components such as mirror, lens and optic fiber are arranged in a standard specimen stage of JEOL TEM so that it could maximize the collection of the emitted light from a sample.

A liquid nitrogen cooling finger was embedded into the TEM-CL stage, which can maintains the temperature of the sample at 150K to improve CL emission efficiency and reduce the carrier recombination diffusion length. Through an optical fiber, the collected light was transmitted to the light detection part which has a spectrometer and a charge-coupled device (CCD). We used an all-in-one spectrometer of Ocean Optics QE56000 model equipped with a CCD located at the end of the optical bench. With a grating of 600 mm^{-1} groove density and a fixed entrance slit (size: 200μm), the spectral resolution of the spectrometer is 3.13nm at 400nm.

TEM-CL experiments are performed with a JEOL 2010F TEM at 120keV accelerating voltage and the electron current density of 50pA/cm^2. To acquire 2-dimenstional data sets of the CL spectra, the focused electron beam was scanned onto the area of interest using an external scanning unit of Oxford instrument (SEMI-STEM).

TEM samples of InGaN QW were prepared by mechanical polishing followed by ion milling of 3.5 kV Ar^+ ions (Gatan PIPS). Weak beam dark

field (WBDF) images and STEM images were taken by a Tecnai F20 TEM from the same area of CL spectra measured.

InGaN/GaN QW samples were prepared by conventional low pressure metal-organic chemical vapor deposition (MOCVD) method. The sample consists of a 3 μm-thick GaN layer grown on (0001) sapphire substrate and three period InGaN (3nm)/GaN (20nm) multiple quantum wells (MQWs) capped with a 150 nm-thick GaN layer. Trimethylgallium (TMGa), trimethylindium (TMIn) and ammonia (NH_3) were used as Ga, In and N sources and hydrogen as carrier gas. Growth temperature of the InGaN and GaN layer is 740 ^oC and 1040 ^oC, respectively.

3. 3. 3. Results and discussions

Figure 3.3.2 shows a plan-view annular dark field (ADF) STEM image of the InGaN/GaN multiple quantum well structure. Because the diffraction contrast is reduced in STEM images, the figure clearly shows the location of the threading dislocations because the diffraction contrast is reduced in STEM images. So, it is easy to match the CL peak wavelength map with dislocations.

Figure 3.3.3 is a overlapped image of a CL wavelength map on the ADF STEM image of the InGaN/GaN multiple quantum wells structure. At the dislocated region with red dotted circles, the peak wavelength of the InGaN active layers is blue-shifted. Although the blue-shift regions are not exactly the same region of dislocated region, tendency of the blue-shift of the peak wavelength is shown in the dislocated region. The blurred distribution of the blue-shifted region is came from the fact that the InGaN active layers are composed of three InGaN quantum wells. And diffusion of the carriers also blur the blue-shifted wavelength region.

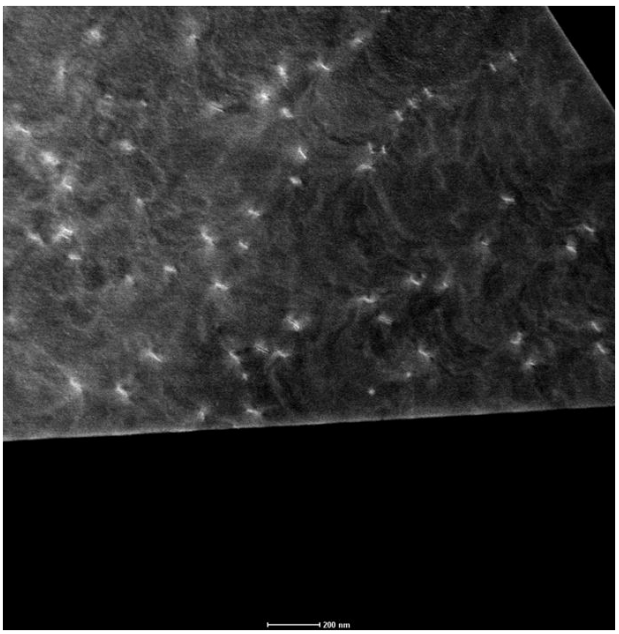

Figure 3.3.2. Plan-view annular dark field (ADF) STEM image of the InGaN/GaN multiple quantum well structure.

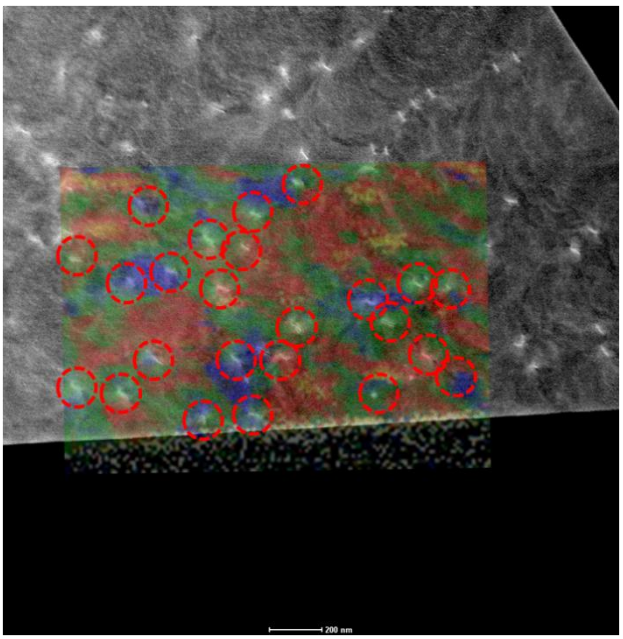

Figure 3.3.3. Overlapped image of a CL wavelength map on the ADF STEM image of the InGaN/GaN multiple quantum wells structure.

To clarify the relations between the dislocations with the peak wavelength shift, we conduct measurements of CL emission with the cross-sectional TEM specimens. Figure 3.3.4 (a) and (b) show weak beam dark field images of a cross-sectional TEM specimen of the InGaN/GaN multiple quantum wells structure with two beam condition of g(0002) and 2g(-4220), respectively. Most of the dislocations treads the InGaN active layers. At the region with square, we taken the CL emission. Figure 3.3.5 shows a overlapped image of the peak wavelength map of InGaN layer on the weak beam dark field image of 2g(-4220) two beam condition. In the Figure xxxx, regions where penetrated by dislocations have blue-shifted CL peak wavelength. Therefore, it is clear that the blue-shift of the CL peak wavelength of the InGaN active layers is originated from the threading dislocations. In other words, ridges in the bandgap plot of InGaN layers (Figure 3.3.6) are region with threading dislocations.

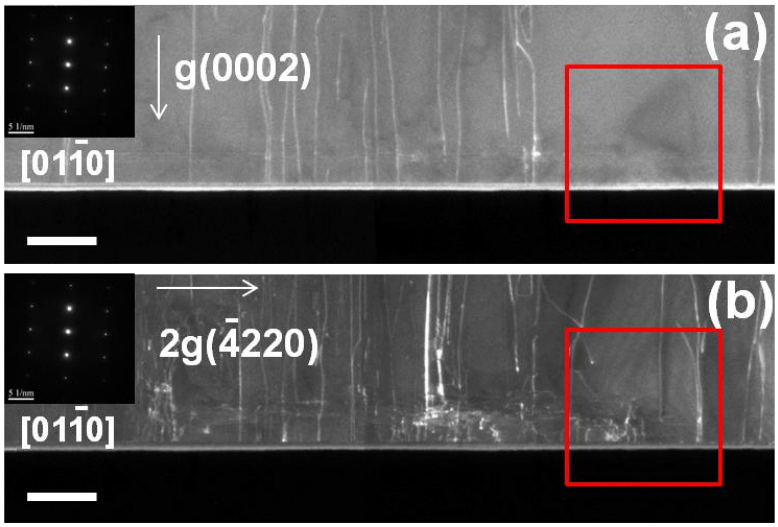

Figure 3.3.4 (a) and (b). Weak beam dark field images of a cross-sectional TEM specimen of the InGaN/GaN multiple quantum wells structure with two beam condition of (a) g(0002) and (b) 2g(-4220), respectively.

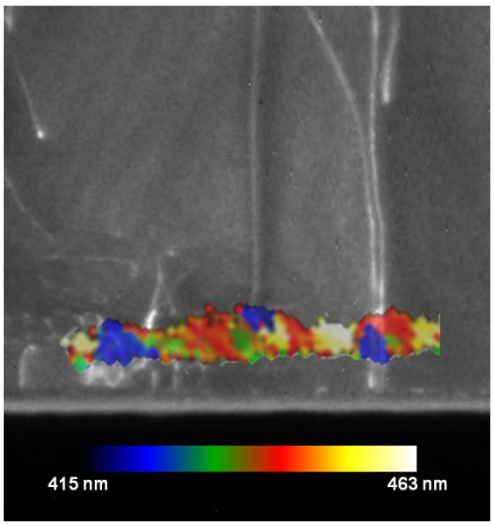

Figure 3.3.5. Overlapped image of the peak wavelength map of InGaN layer on the weak beam dark field image of 2g(-4220) two beam condition.

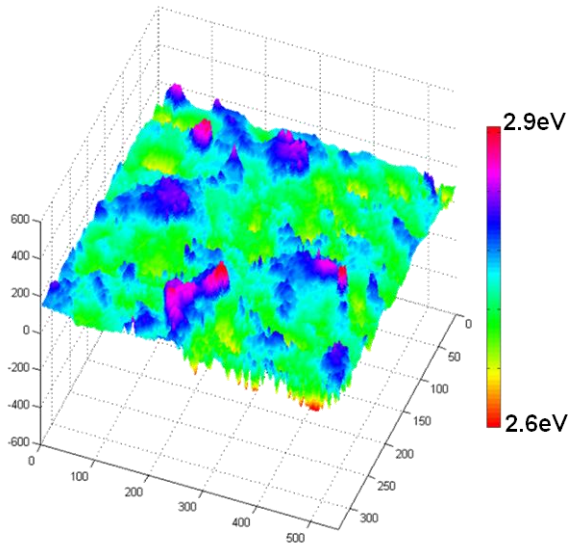

Figure 3.3.6. Distribution of the bandgap converted from the wavelength variations using the wavelength and photon energy relationship.

Based on these observations, we proposed that the defect insensitivity of the radiative recombination probability of the InGaN active layers is due to the anti-localization of carriers at the region where penetrated by dislocations (Figure 3.3.7). The threading dislocations increase the bandgap energy of the InGaN active layers and the carriers cannot easily locate at the dislocated region. In other words, dislocations in the light emitting devices using the InGaN active layers make energy barriers in the active layers. When the devices working, therefore, injected carriers in the InGaN active layers see the energy barriers at the dislocated region and consequently they will actively recombine at the other regions which have low bandgap energy.

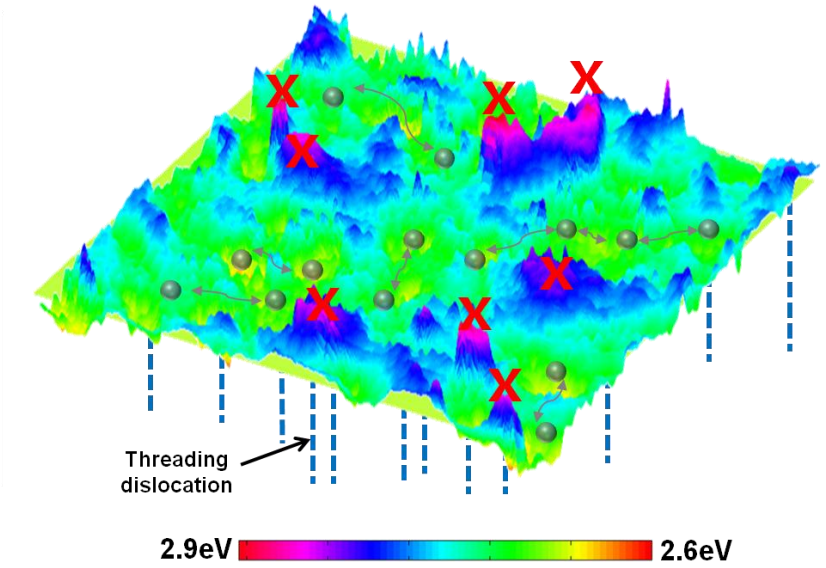

Figure 3.3.7. A schematic view of anti-localization of carriers at the region where penetrated by dislocations.

3. 3. 4. Summary

In this study, we show that the bandgap energy of the InGaN active layers is increased in the regions where dislocations penetrate the active layers by cross-sectional TEM observations and cathodoluminescence analysis. Therefore, dislocations in the blue-light emitting diodes devices with the InGaN active layers self-screen the carriers in the InGaN active layers. When the devices working, therefore, injected carriers in the InGaN active layers see the energy barriers at the dislocated region and consequently they will actively recombine at the other regions which have low bandgap energy.

Chapter 4. Conclusion

Cathodoluminescence analysis of III-nitride materials (GaN and InGaN) was conducted in a transmission electron microscope by using a home-built light collectable TEM stage. Optical components such as mirror, lens and optical fibers are carefully arranged in a standard TEM stage to make effective CL light collection. Also, the light collectable TEM stage was combined with a liquid nitrogen cooling system. Combination with the cooling system make increased light emitting efficiency and give us more detailed spectral information of the sample.

Optical properties of the threading dislocations in the GaN thin films were investigated by the TEM-CL system. We can show the band edge emission monochromatic spectral map. From these maps, we can know that he threading dislocations act as non radiative recombination center for band edge emission. Also, we generated the yellow band spectral maps. It reveals that the yellow band emission is not originated from the threading dislocations. We also showed that doping of the GaN films change the defects state of dislocations by the yellow band emission spectral maps.

Cathodoluminescence emission of the InGaN multiple-quantum wells active layers for blue-light emitting diodes was investigated. The non-uniform radiative recombination probability of the carriers in the InGaN active layers is shown by the panchromatic spectral image of the InGaN layers. This non-uniform distribution of the light emission is come from the non-

uniformity of In concentration in the InGaN active layers. The “in-plane” wavelength map of band edge emission peak of InGaN layers also shows the inhomogeneity of the In concentration. From the band-gap energy plot, we can know that the carriers maybe concentrated at the hump regions in the band-gap energy plot. So, the probability of the radiative recombination is increased at that region.

Cross-sectional TEM observations and cathodoluminescence analysis reveals that the bandgap energy of the InGaN active layers is increased in the regions where dislocations penetrate the active layers. The threading dislocations in the blue-light emitting diodes devices with the InGaN active layers self-screen the carriers in the InGaN active layers. When the devices working, injected carriers in the InGaN active layers see the energy barriers at the dislocated region and consequently they will actively recombine at the other regions which have low bandgap energy.

References

1. Yacobi, F. G. Cathodoluminescence Microscopy of Inorganic Solids, Plenum Press, 1990.

2. Schubert, E. F. Light-Emitting Diodes (second edition), Cambridge University Press, 2006.

3. Morkoc, H. & Mohammad, S. N. High-Luminosity Blue and Blue-Green Gallium Nitride Light-Emitting-Diodes. Science 267, 51-55 (1995).

4. Ponce, F. A. & Bour, D. P. NItride-based semiconductors for blue and green light-emitting devices. Nature 386, 351-359 (1997).

5. Chichibu, S. F. et al. Origin of defect-insensitive emission probability in In-containing (Al, In, Ga) N alloy semiconductors. Nature Materials 5, 810-816 (2006).

6. Nakamura, S. The roles of structural imperfections in InGaN-Based blue light-emitting diodes and laser diodes. Science 281, 956-961 (1998).

7. Nakamura, S. & Mukai, T. High-Quality Ingan Films Grown on Gan Films. Japanese Journal of Applied Physics Part 2-Letters 31, L1457-L1459 (1992).

8. Nakamura, S., Mukai, T., Senoh, M., Nagahama, S. & Iwasa, N. Inxga(1-X)N/Inyga(1-Y)N Superlattices Grown on Gan Films. Journal of Applied

Physics 74, 3911-3915 (1993).

9. Chichibu, S., Azuhata, T., Sota, T. & Nakamura, S. Spontaneous emission of localized excitons in InGaN single and multiquantum well structures. Applied Physics Letters 69, 4188-4190 (1996).

10. Chichibu, S. F. et al. Optical properties of InGaN quantum wells. Materials Science and Engineering B-Solid State Materials for Advanced Technology 59, 298-306 (1999).

11. Chichibu, S. F. et al. Effective band gap inhomogeneity and piezoelectric field in InGaN/GaN multiquantum well structures. Applied Physics Letters 73, 2006-2008 (1998).

12. Chichibu, S., Wada, K. & Nakamura, S. Spatially resolved cathodoluminescence spectra of InGaN quantum wells. Applied Physics Letters 71, 2346-2348 (1997).

13. Duxbury, N. et al. Indium segregation in InGaN quantum-well structures. Applied Physics Letters 76, 1600-1602 (2000).

14. Gerthsen, D. et al. Composition fluctuations in InGaN analyzed by transmission electron microscopy. Physica Status Solidi a-Applications and Materials Science 177, 145-155 (2000).

15. Smeeton, T. M., Kappers, M. J., Barnard, J. S., Vickers, M. E. &

Humphreys, C. J. Electron-beam-induced strain within InGaN quantum wells: False indium "cluster" detection in the transmission electron microscope. Applied Physics Letters 83, 5419-5421 (2003).

16. Galtrey, M. J. et al. Three-dimensional atom probe studies of an InxGa1-xN/GaN multiple quantum well structure: Assessment of possible indium clustering. Applied Physics Letters 90 (2007).

17. Graham, D. M. et al. Optical and microstructural studies of InGaN/GaN single-quantum-well structures. Journal of Applied Physics 97 (2005).

18. Kwon, S. Y. et al. Optical and microstructural studies of atomically flat ultrathin In-rich InGaN/GaN multiple quantum wells. Journal of Applied Physics 103 (2008).

19. Sugahara, T. et al. Direct evidence that dislocations are non-radiative recombination centers in GaN. Japanese Journal of Applied Physics Part 2-Letters 37, L398-L400 (1998).

20. Yamamoto, N. et al. Cathodoluminescence characterization of dislocations in gallium nitride using a transmission electron microscope. Journal of Applied Physics 94, 4315-4319 (2003).

21. Albrecht, M. et al. Carrier recombination at single dislocations in GaN measured by cathodoluminescence in a transmission electron microscope.

Journal of Applied Physics 92, 2000-2005 (2002).

22. Arslan, I., Bleloch, A., Stach, E. A. & Browning, N. D. Atomic and electronic structure of mixed and partial dislocations in GaN. Physical Review Letters 94 (2005).

23. Cheong, M. G. et al. Effects of growth interruption on the optical and the structural properties of InGaN/GaN quantum wells grown by metalorganic chemical vapor deposition. Journal of Applied Physics 90, 5642-5646 (2001).

24. Chung, S. J. et al. Emission mechanism of the yellow luminescence in undoped GaN. Journal of the Korean Physical Society 37, 1003-1006 (2000).

25. Chuo, C. C., Lee, C. M., Nee, T. E. & Chyi, J. I. Effects of thermal annealing on the luminescence and structural properties of high indium-content InGaN/GaN quantum wells. Applied Physics Letters 76, 3902-3904 (2000).

26. Fleischer, K. et al. Depth profiling of GaN by cathodoluminescence microanalysis. Applied Physics Letters 74, 1114-1116 (1999).

27. Follstaedt, D. M., Missert, N. A., Koleske, D. D., Mitchell, C. C. & Cross, K. C. Plan-view image contrast of dislocations in GaN. Applied Physics Letters 83, 4797-4799 (2003).

28. Grazzi, C. et al. Optoelectronic properties of GaN epilayers in the region

of yellow luminescence. Journal of Applied Physics 100 (2006).

29. Ho, I. H. & Stringfellow, G. B. Solid phase immiscibility in GaInN. Applied Physics Letters 69, 2701-2703 (1996).

30. Hofmann, D. M. et al. Properties of the yellow luminescence in undoped GaN epitaxial layers. Physical Review B 52, 16702-16706 (1995).

31. Ino, N. & Yamamoto, N. Low temperature diffusion length of excitons in gallium nitride measured by cathodoluminescence technique. Applied Physics Letters 93 (2008).

32. Jeong, M. S. et al. Spatial variation of photoluminescence and related defects in InGaN/GaN quantum wells. Applied Physics Letters 79, 3440-3442 (2001).

33. Ko, T. S. et al. InGaN/GaN nanostripe grown on pattern sapphire by metal organic chemical vapor deposition. Applied Physics Letters 90 (2007).

34. Lei, H. P., Chen, J. & Ruterana, P. Influences of the biaxial strain and c-screw dislocation on the clustering in InGaN alloys. Journal of Applied Physics 108 (2010).

35. Lim, S. K. et al. Direct Correlation between Structural and Optical Properties of III-V Nitride Nanowire Heterostructures with Nanoscale Resolution. Nano Letters 9, 3940-3944 (2009).

36. Mitsui, T., Yamamoto, N., Tadokoro, T. & Ohta, S. Cathodoluminescence image of defects and luminescence centers in ZnS/GaAs(100). Journal of Applied Physics 80, 6972-6979 (1996).

37. Miyajima, T. et al. Threading dislocations and optical properties of GaN and GaInN. Physica Status Solidi B-Basic Research 228, 395-402 (2001).

38. Nakaji, D., Grillo, V., Yamamoto, N. & Mukai, T. Contrast analysis of dislocation images in TEM-cathodoluminescence technique. Journal of Electron Microscopy 54, 223-230 (2005).

39. Narukawa, Y. et al. Role of self-formed InGaN quantum dots for exciton localization in the purple laser diode emitting at 420 nm. Applied Physics Letters 70, 981-983 (1997).

40. Ohno, Y. In-situ analysis of optoelectronic properties of twin boundaries in AlGaAs by polarized cathodoluminescence spectroscopy in a TEM. Journal of Electron Microscopy 59, S141-S147 (2010).

41. Phillips, M. R., Telg, H., Kucheyev, S. O., Gelhausen, O. & Toth, M. Cathodoluminescence efficiency dependence on excitation density in n-type gallium nitride. Microscopy and Microanalysis 9, 144-151 (2003).

42. Polenta, L., Castaldini, A. & Cavallini, A. Defect characterization in GaN: Possible influence of dislocations in the yellow-band features. Journal of

Applied Physics 102 (2007).

43. Rosner, S. J., Carr, E. C., Ludowise, M. J., Girolami, G. & Erikson, H. I. Correlation of cathodoluminescence inhomogeneity with microstructural defects in epitaxial GaN grown by metalorganic chemical-vapor deposition. Applied Physics Letters 70, 420-422 (1997).

44. Saghai, H. R., Asgari, A., Nejad, H. B. A. & Rostami, A. A study in optical properties of AlGaN/GaN pyramid and prism-shape quantum dots. Physica E-Low-Dimensional Systems & Nanostructures 41, 245-253 (2008).

45. Shalish, I. et al. Yellow luminescence and related deep levels in unintentionally doped GaN films. Physical Review B 59, 9748-9751 (1999).

46. Shim, H. W. et al. Influence of the quantum-well shape on the light emission characteristics of InGaN/GaN quantum-well structures and light-emitting diodes. Applied Physics Letters 81, 3552-3554 (2002).

47. Suski, T. et al. Mechanism of Yellow Luminescence in Gan. Applied Physics Letters 67, 2188-2190 (1995).

48. Watanabe, K. et al. Atomic-scale strain field and In atom distribution in multiple quantum wells InGaN/GaN. Applied Physics Letters 82, 715-717 (2003).

49. Wu, X. H. et al. Structural origin of V-defects and correlation with

localized excitonic centers in InGaN/GaN multiple quantum wells. Applied Physics Letters 72, 692-694 (1998).

50. Wu, X. H. et al. Dislocation generation in GaN heteroepitaxy. Journal of Crystal Growth 189, 231-243 (1998).

51. Xu, J. et al. Cathodoluminescence study of InGaN/GaN quantum-well LED structures grown on a Si substrate. Journal of Electronic Materials 36, 1144-1148 (2007).

52. Yoo, H. et al. Microstructures of GaN Thin Films Grown on Graphene Layers. Advanced Materials 24, 515-+ (2012).

Curriculum Vitae

Sung-Dae Kim

Ph.D. Candidate

Department of Materials Science and Engineering

Seoul National University

31-411, Gwan-ak ro 599, Dae-hak dong, Gwan-ak gu,

Seoul, Republic of Korea

Tel:+82-2-878-5010 Fax:+82-2-878-5010

e-mail : sdkim57@snu.ac.kr sdkim57v@gmail.com

QUALIFICATIONS

- Dexterous in microstructure analysis using various instruments such as (S)TEM, SEM, EDS, EELS, FIB and XRD
- Widely experienced in *in-situ* electron microscopy
- Dexterous in apparatus set up for *in-situ* transmission electron microscopy (home built heating stage, home built electrical probing stage, home built liquid nitrogen cooling stage, home built TEM-CL detection systems)
- Acquainted with vacuum systems of electron and ion beam instruments

EDUCATION

Integrated MA/Ph.D., Department of Materials Science and Engineering, Seoul National University, Seoul, Republic of Korea (March 2006 ~)

B.S., Materials Science and Engineering, Seoul National University Seoul, Republic of Korea (March 2001 ~ February 2006)

RESEARCH AREAS

- ***TEM-Cathodoluminescence characterization***
  - ***TEM-CL System Development***

    Development of a home-built light detection system attached to dedicated CL TEM

    Development of a home-built light collecting TEM specimen stage

    Development of a home-built light collecting TEM specimen stage combined with liquid nitrogen cooling system
  - ***TEM-CL analysis of semiconducting materials***

    TEM-CL analysis of threading dislocations in the GaN thin films

    TEM-CL analysis of In composition fluctuation in the InGaN quantum well layers in InGaN/GaN based blue light emitting diodes

    TEM-CL analysis of nanostructure materials such as $CdS@SnO_2$ nano-rods, ZnO nano-wires
- ***In-situ transmission electron microscopy***
  - ***In-situ TEM specimen stage development***

Development of a home-built heating stage

Development of a home-built electrical probing stage

- ***In-situ TEM analysis of various materials***

  In-situ heating experiment of Au/Ni/AuGe/GaAs Ohmic structure

  In-situ heating experiment of grain growth of advanced steels and magnesium composites.

  In-situ electrical probing experiment of materials for memory devices (ReRAM, PcRAM)

  In-situ tensile experiment of carbon nano-tubes (using an *in-situ* probing stage)

- ***Microstructure analysis using electron microscopes***
  - Microstructure analysis of precipitates in an aluminum matrix metal composite reinforced by icosahedral quasi-crystalline particles
  - TEM analysis of sub-grain boundaries in abnormally growing Goss grains in Fe-Si steel
  - Microstructure analysis of Twin-Induced Plasticity (TWIP) steel
  - Measurement of tensile strength of a carbon micro-fiber using a home built nano-manipulation system in SEM
  - Real-time observation of defects generation in Na- alumina by electron beam irradiation
  - Microstructure analysis of surface morphology of thermally oxidized silicon nano-wires

- Microstructure analysis of graphene films grown at near room-temperature
- Microstructure analysis of GaN based LED
- Microstructure analysis of ZnO-MgO heterostructre nano particle phosphor

EXPERIMENTAL SKILLS

- ***Transmission Electron Microscope (TEM) Operation***
  - Instrument: JEM 2010F TEM (JEOL), JEM 2100F with Cs-corrector TEM (JEOL), JEM 3000F(JEOL), JEM 200CX (JEOL), JEM 1010 (JEOL), F20 (Tecnai)
- ***Scanning Electron Microscope (SEM) Operation***
  - Instrument: JSM-6390LV (JEOL), JSM-5600 (JEOL), JSM-5200 (JEOL), JSM-6390 (JEOL)
- ***X-ray Diffractometer (XRD) Operation***
  - Instrument: X'pert Pro (PANalytical)
- ***Focused Ion Beam (FIB) Operation***
  - Instrument: SMI3050SE (SII Nanotechnology)

- ***EM simulation tools***
  - JEMS (Java version of the EMS electron microscopy simulation program), DM (Desktop Microscopist for Mac PC), Crystal Maker

- ***Image editing tools***
  - ImageJ (image stack generating and editing), IMOD (3D tomography), DM (Gatan), VirtualDub (movie editing), Camtasia (movie making)
- ***Instrument design tools***
  - Autodesk Inventor (3D design), Autodesk AutoCAD (2D design)
- ***Set up and Operation of vacuum chamber***
  - Set up a UHV chamber with RP, Turbo pump, and IGP (Ion Getter Pump) to 10^{-10} Torr vacuum range
  - Set up a multi-functional vacuum chamber for vacuum annealing and thermal evaporation

AWARDS

- Scholarship of Academic Excellence from Seoul National University, 2006
- MSA (Microscopy Society of America) Poster Award (Physical Science ***1st Prize***), Microscopy and Microanalysis 2007, 2007

PATENTS

- Dong-Su Ko, Young-Woon Kim, **Sung-Dae Kim**, Tae-Young Ahn, '다중 미세조작이 가능한 탐침을 구비하는 홀더 장치 및 측정 시스템', 10-1033352 (registration), 2011 (Korean Patent)

- Young-Woon Kim, Bon-Woong Koo, **Sung-Dae Kim**, '집게를 구비하는 극미세 조작 전자현미경 스테이지', 10-2012-0065037 (application), 2012 (Korea patent)
- Young-Woon Kim, Bon-Woong Koo, **Sung-Dae Kim**, '집게를 구비하는 극미세 조작가능한 인장 전자현미경 스테이지', 10-2012-0065038 (application), 2012 (Korea patent)
- **Sung-Dae Kim**, Young-Woon Kim, Tae-Young Ahn, '집광장치를 구비하는 전자현미경 홀더 장치', 10-2012-0109933 (application), 2012 (Korea patent)

LIST OF PUBLICATIONS (SCI JOURNALS)

---

1. Dong-Su Ko, Young Min Park, **Sung-Dae Kim**, Young-Woon Kim, "Effective removal of Ga residue from focused ion beam using a plasma cleaner", *Ultramicroscopy* 107, 368–373 (2007)

2. Hyung-Ki Park, **Sung-Dae Kim**, Seung-Chul Park, Jong-Tae Park, Nong-Moon Hwang, "Sub-boundaries in abnormally growing Goss grains in Fe–3% Si steel", *Scripta Mater.* 62, 376–378 (2010)

3. Tae Kenny Yoonki Hwang, **Sung-Dae Kim**, Young-Woon Kim, Woong-Ryeol Yu, " Mechanical characterization of nanofibers using a nanomanipulator and atomic force microscope cantilever in a scanning

electron microscope", *Polym. Test.* 29, 375–380 (2010)

4. **Sung-Dae Kim**, Dong-Su Ko, Woo Kil Jang, Kwang Seon Shin, Young-Woon Kim, “Precipitation hardening through sacrificial phase in aluminum–quasicrystal metal matrix composites”, *Mater. Sci. Eng. A* 528, 4845–4848 (2011)

5. Jiwon Park, **Sung-Dae Kim**, Seung-Pyo Hong, Sung-Il Baik Dong-Su Ko, Choong Yeol Lee, Duk-Lak Lee, Young-Woon Kim, " Quantitative measurement of cementite dissociation in drawn pearlitic steel ", *Mater. Sci.Eng. A* 528, 4947–4952 (2011)

6. Jinsung Kwak, Jae Hwan Chu, Jae-Kyung Choi, Soon-Dong Park, Heungseok Go, Sung Youb Kim, Kibog Park, **Sung-Dae Kim**, Young-Woon Kim, Euijoon Yoon, Suneel Kodambaka, Soon-Yong Kwon, " Near room-temperature synthesis of transfer-free graphene films ", *Nature. Commun.* 3:645, (2012)

7**.** Seulah Lee, Ja Hoon Koo, Jungmok Seo, **Sung-Dae Kim**, Kwang Hyun Lee, Seongil Im, Young-Woon Kim, Taeyoon Lee, “The effects of surface modification on the electrical properties of p–n+ junction silicon nanowires grown by an aqueous electroless etching method”, *J. Nanopart. Res.* 14:840, (2012)

8. Dong-Su Ko, Seong-Il Kim, Tae-Young Ahn, **Sung-Dae Kim**, Young-Hwa Oh, Young-Woon Kim, " Effect of the electrode materials on the resistive switching of Ti4O7", *Appl. Phys. Lett* 101, 053502 (2012)

9. Heungseok Go, Jinsung Kwak, Youngeun Jeon, **Sung-Dae Kim**, Byung Cheol Lee, Hyun Suk Kang, Jae-Hyeon Ko, Nam Kim, Bum-Kyu Kim, Jung-Woo Yoo, Sung Youb Kim, Young-Woon Kim, Soon-Yong Kwon, Kibog Park, "Low-temperature formation of epitaxial graphene on 6H-SiC induced by continuous electron beam irradiation", *Appl. Phys. Lett* 101, 092105 (2012)

10. Jun Hee Choi, Ho Young Ahn, Yun Sung Lee, Kyungwoo Park, Tae-Ho Kim, Kyung Sang Cho, Chan Wook Baik, Sun Il Kim, Hyobin Yoo, Eun Hong Lee, Byoung Lyong Choi, **Sung-Dae Kim**, Young-Woon Kim, Miyoung Kim, Sungwoo Hwang, "GaN light-emitting diodes on glass substrates with enhanced electroluminescence", *J. Mater. Chem.*, in press

11. Jae-Kyung Choi, Jae-Hoon Huh, **Sung-Dae Kim**, Daeyoung Moon, Duhee Yoon, Kisu Joo, Jinsung Kwak, Jae Hwan Chu, Sung Youb Kim, Kibog Park, Young-Woon Kim, Euijoon Yoon, Hyeonsik Cheong, Soon-Yong Kwon, "One-Step Graphene Coating of Heteroepitaxial GaN Films", *Nanotechnology*, in press

Abstract (in Korean)

가속된 전자가 물체에 조사되었을 때 다양한 이차신호 (후방 산란 전자, 이차 전자, 특성 X-선 등)가 발생한다. 이와 같은 이차신호는 물질의 구조적, 화학적, 전기적 특성에 관한 정보를 포함하고 있다. 전자현미경은 물체에 전자 빔을 조사함으로써 이와 같은 이차신호를 발생시키고 또한 감지하여 물질의 특성에 관한 정보를 제공한다. 이와 같은 다양한 이차신호 중, 음극형광 (Cathodoluminescence) 분석법은 적외선, 가시광선, 자외선 영역의 빛을 감지하고 분석하여 물질의 밴드갭 에너지 구조에 관한 정보를 제공한다. 본 연구에서는 투과전자현미경을 활용한 음극형광 분석법을 개발하여 물체의 내부 구조 (microstructure)와 광학적 특성의 연관성을 파악하고자 하였다. 우선 전자 빔과 시편의 반응에 의해 발생하는 빛을 수집할 수 있는 시스템을 개발하였다. 이를 위해 집광을 위한 요소 (미러, 렌즈, 광섬유 등)를 투과전자현미경 시편 스테이지에 배치한 '집광 가능한 투과전자현미경 시편 스테이지'를 개발하였다. 또한 음극형광에 의해 발생하는 빛의 양을 증가시키고 분광 분해능을 향상시키기 위해 액화질소를 활용한 냉각 시스템을 '집광 가능한 투과전자현미경 시편 스테이지'에 장착하였다.

이와 같이 개발된 투과전자현미경을 활용한 음극형광 분석 시스템을 활용하여 GaN 기반의 발광소자 내에 존재하는 미세구조의 광학적 특성을 분석하는 연구를 진행하였다. 우선 음극형광 분석 기법을 활용하여 GaN 박막 내에 존재하는 전위의 광학적 특성을 파악하고자

하였다. 일반적인 GaN 박막은 사파이어 등의 이종 기판에 성장시키는데, 이때 기판과 박막의 격자 상수 차이에 의해 발생하는 응력을 해소하기 위해 전위가 생성된다. GaN 박막 내에 존재하는 이 같은 전위의 band edge emission 음극형광 분광 이미지 (monochromatic, panchromatic spectral image)를 분석한 결과, 전위는 GaN 박막 내에서 비발광 부위 (non radiative recombination center)인 것을 확인할 수 있었다. 또한 전위가 일정하게 배열된 형태를 갖는 경각입계 (low-angle grain boundary)의 경우 또한 비발광 부위로 작용하여 소자의 발광 효율 저하의 원인이 될 수 있음을 확인하였다. 이와 더불어 GaN의 음극형광 스펙트럼에서 나타나는 yellow band emission에 관한 분석도 진행하였다. Yellow band emission 음극형광 분광 이미지 (panchromatic spectral image)를 분석한 결과, GaN 박막의 도핑 여부에 따라 전위 부근에서의 발광 특성이 달라짐을 확인하였다. 이를 통하여 yellow band emission이 전위에 기인하는 것이 아님을 간접적으로 확인할 수 있었다.

또한 투과전자현미경을 활용한 음극형광 분석 기법을 활용하여 단파장 발광소자에 주로 활용되는 InGaN 발광층의 밴드갭 에너지 분포에 관한 연구를 진행하였다. III-nitride 물질을 기반으로 하는 발광소자의 경우 높은 전위 밀도를 가짐에도 불구하고 높은 발광효율을 나타내는 것으로 알려져 있다. 그 동안 이러한 현상을 설명하기 위해 많은 연구가 진행되어 왔는데, 대부분의 연구에서는 이 같이 높은 발광효율은 InGaN 발광층에서의 In 조성 불균일에 따른 밴드갭 에너지의

국부적 저하에서 기인한다고 보고하고 있다. 본 연구에서는 음극형광 분석을 통해 이와 같은 밴드갭 에너지의 불균일을 미세구조적인 증거를 제시하였다. 또한 그 동안 명확히 제시되지 못했던 전위가 InGaN 물질의 발광특성에 미치는 영향에 대한 연구를 진행하였다. 음극형광 분석을 통한 밴드갭 에너지 분포를 확인한 결과, 전위가 InGaN 발광층을 관통하는 부위에서 밴드갭 에너지가 증가됨을 확인하였다. 즉, 전위가 관통하는 부위에서 밴드갭 에너지 barrier가 형성되어 InGaN 층 내에 속박된 carrier들이 밴드갭 에너지가 증가된 부위에 위치할 확률이 낮아지게 된다. 따라서 이 같은 carrier들의 InGaN 발광층 내에서 전위에 의한 비발광 결합 확률의 저하가 InGaN 발광층을 갖는 소자의 높은 원인 중 하나임을 확인할 수 있다.

주요어 : 음극형광, 투과전자현미경, 전위, 발광 특성, 질화갈륨, 인듐질화갈륨갈륨, 발광소자, 밴드갭 에너지

학 번 : 2006-20822

김 성 대

감사의 글

관악에서의 짧고도 긴 학위기간 동안에 많은 도움을 주신 분들과 기쁨과 슬픔을 함께 나누었던 동료들, 그리고 제가 여기까지 올 수 있도록 허락해 준 사랑하는 가족들에게 감사의 말씀을 올립니다.

우선, 저를 연구실의 일원으로 허락해 주시고 학위기간 동안 부족한 저를 여기까지 올 수 있도록 지도해 주신 저의 '교수님' 김영운 교수님께 감사의 말씀을 드립니다. 교수님께서 제게 주신 많은 기회와 가르침을 잊지 않으며, 사회에 나가서도 교수님과 연구실이 쌓은 명성에 흠이 되지 않도록 노력하겠습니다. 바쁘신 와중에도 저의 학위 논문의 심사 위원장을 맡아 주시고 실험 결과 해석에 깊이를 더해 주신 윤의준 교수님과 학위기간 동안 언제나 친절히 대해 주시고 연구적인 측면에서 새로운 해석을 고민하게 해 주신 김미영 교수님께도 감사 드립니다. 그리고 부족한 저의 졸업 논문을 지도해 주시고 따뜻한 조언을 아끼지 않으셨던 양철웅 교수님과 저의 연구 인생에 대한 많은 조언을 해 주신 권순용 교수님께 진심으로 감사의 말씀을 올립니다.

대학원 생활이라는 길고 외로운 길에 기쁨과 슬픔을 함께 나눈 저의 소중한 사람들에게도 감사의 말을 전합니다. 연구의 길에 처음 들어섰을 때 저를 혹독하게 단련해 주셨던, 이제는 연구라는 이 길을 기쁘게 함께 하고 있는 고동수 박사님께 진심으로 고맙다는 말씀을 전합니다. 동수형이 없었다면 아마 저는 연구자로서 지금보다 더욱 더 부족한 사람이었을 것이라 고백합니다. 그리고 실험실의 기둥으로서 많은 기반을 미리

닦아주시고 실험실원들의 롤모델이 되어주신 백성일 박사님께도 멀리서나마 감사의 말씀을 드립니다. 힘이 들 때 진심으로 위로해 주고 기쁠 때 함께 웃어주던 영화누나에게 진심으로 감사의 말을 전합니다. 누나가 있어 학위 기간의 마지막을 견뎌낼 수 있었어요. 고마워요. 그리고 나이 어린 철없는 선배인 저를 믿고 함께 여기까지 와 준 본웅형에게도 고맙다는 말을 전합니다. 형, 결혼 미리 축하하고 형도 곧 이 글을 쓰게 될 거라 믿어 의심치 않아요. 힘내요. 저의 대학원 생활 동안에 생사고락을 함께한 안태영, 김성일 에게도 평소에 하지 못했던 고맙다는 말을 이렇게나마 전합니다. 부족한 형 믿고 잘 따라줘서 고마워. 너희들이 없었으면 내가 여기까지 오지 못했을거야. 내 맘 알지? 그리고 동갑내기 친구로서 내 부족함을 많이 채워 준 홍승표에게도 감사의 말을 전합니다. 승표야, 네가 있어 언제나 든든했다. 고맙다. 저의 학위에 절대적인 도움을 준 언제나 성실한 이종환에게도 감사의 말을 전합니다. 종환아, 너 덕분에 졸업한다. 또한 많은 시간을 함께하지는 못하겠지만 종환이와 함께 저의 뒤를 이어줄 미향에게도 감사의 말을 전합니다. 이 외에도 지금은 연구실을 떠나 사회에서 훌륭한 몫을 해 내고 있는 희석형, 향숙누나, 영민형, 이호형, 웅표, 영진이와 멀리서 고생하고 있을 하나뿐인 동기 지원이에게도 감사의 말을 전하며 다들 건승하길 빕니다.

또한, 저의 학위기간 중 희로애락을 격하게 함께한 소울 메이트 장재혁 박사님과 대학원 기간 동안의 고민을 함께 나눈 컴퓨터 두뇌 종명형, 스마트 가이 권지환 박사에게도 감사의 말을 전합니다. 그리고 대학원

생활에 많은 추억을 함께한 원자및전자구조 연구실 덕황, 승진, 근수, 아람, 민관, 진호, 효빈, 상문, 승용, 장현에게 감사의 말을 전합니다. 또한 저의 졸업에 지대한 도움을 준 비운의 천재 문대영 학생과 울산과학기술대학교 최재경 학생에게도 진심으로 감사의 말을 전합니다. 이 외에도 학위의 마지막을 함께 불태운 임재혁 박사와 대학원 생활 중 좋은 추억 함께 나눈 UP 맴버 문수, 효진에게도 고맙다는 말을 전합니다.

대학 시절부터 저와 함께 해준 경열형, 철홍형, 선호형, 율형, 상민, 종학, 혜연, 승의 이하 활빈당 동지들에게 감사의 마음을 전합니다. 그리고 자주는 못 보지만 늘 가까이 있는 자발회 동헌, 규도, 승준, 병제, 정민에게도 고마움의 마음을 전합니다.

그리고 지금까지 저를 믿고 기다려 준 사랑하는 가족들에게 감사의 말을 올립니다. 제가 마음 편안히 공부를 계속 할 수 있게 해 준 저의 형과 형수님 그리고 곧 세상에 나올 반디에게 고마움의 마음을 전하며 더욱 행복하길 간절히 바랍니다. 그리고 서울 타향살이에 힘들 때 마다 편안한 안식처가 되어주신 작은아버지, 작은어머님께 감사의 말씀을 올립니다. 그리고 내 인생을 관통하는 정신적 동반자 일중이, 곧 선생님이 될 효중이에게도 감사의 마음을 전합니다. 그리고 제가 흔들리지 않고 지금까지 올 수 있게 해 주신 하늘에 계신 할아버지, 할머니께도 마음속 깊이 감사의 말씀을 올립니다.

마지막으로 고마움의 마음을 말로 다 표현할 수 없는 저의 아버지, 어머니께 이 모든 것을 바칩니다. 부모님의 고단한 인생에 저의 이 자그마한 성취가 조금이나마 위로가 되기를 진심으로 바랍니다. 사랑합니다.

2013 년 2 월

관악에서